National Library
of Canada

Acquisitions and
Bibliographic Services Branch

395 Wellington Street
Ottawa, Ontario
K1A 0N4

Bibliothèque nationale
du Canada

Direction des acquisitions et
des services bibliographiques

395, rue Wellington
Ottawa (Ontario)
K1A 0N4

Your file Votre référence

Our file Notre référence

NOTICE

The quality of this microform is heavily dependent upon the quality of the original thesis submitted for microfilming. Every effort has been made to ensure the highest quality of reproduction possible.

If pages are missing, contact the university which granted the degree.

Some pages may have indistinct print especially if the original pages were typed with a poor typewriter ribbon or if the university sent us an inferior photocopy.

AVIS

La qualité de cette microforme dépend grandement de la qualité de la thèse soumise au microfilmage. Nous avons tout fait pour assurer une qualité supérieure de reproduction.

S'il manque des pages, veuillez communiquer avec l'université qui a conféré le grade.

La qualité d'impression de certaines pages peut laisser à désirer, surtout si les pages originales ont été dactylographiées à l'aide d'un ruban usé ou si l'université nous a fait parvenir une photocopie de qualité inférieure.

Canada

New Evidence for Flux Cutting in Type II Superconductors

by

David LeBlanc

Thesis submitted to the University of Ottawa
in partial fulfilment of the requirements
for the degree of Master of Physics

Department of Physics
University of Ottawa

ISBN 0-315-85830-3

Canada

UNIVERSITÉ D'OTTAWA
UNIVERSITY OF OTTAWA

ACKNOWLEDGEMENTS

I would like to express my gratitude to Dr. Marcel A. R. LeBlanc for his excellent guidance, supervision, encouragement and inspiration provided throughout all stages of this project

I would also like to thank the members of both machine and electronics shop for their contributions in the manufacturing and assembling of the setup used in this project.

Finally, I would like to thank my family.

ABSTRACT

We present new evidence for cross flow and cutting of nonparallel flux lines in type II superconductors. A dramatic reversal is observed in the evolution of $B_{z\,hole}$, the axial flux density in the cavity of a hollow cylinder when the magnitude of a helical magnetic field, $\vec{H}_{ext} = \hat{\phi}H_{\phi} + \hat{z}H_{\parallel}$ is increased or decreased along the surfaces of the specimen. This turn around constitutes a 180° degree deviation from the predictions of the "classical" critical state framework (no flux line cutting).

Measurements of the concurrent evolution of $< B_z >_{wall}$, the axial flux density threading the wall of the hollow cylinder, complement the above data. The behaviour of $< B_z >_{wall}$ is also in drastic disagreement with the "classical" picture of "one way" traffic of flux lines dictated solely by the change in magnitude of $\vec{H}_{ext}$. These observations also provide strong support for our interpretation. Our account of these unexpected phenomena is based on the ideas of two way traffic of sublattices of nonparallel flux lines traversing each other via flux line cutting processes.

We briefly review the classical critical state concept. The essential features of the flux cutting process, cross traversal of flux line sheets and attendant "breathing modes are also outlined. Then the Generalized Critical State Model incorporating a phenomenlogical framework based on Maxwell's equations, standard physical constraints and two separate energy dissipation mechanisms is summarized. Finally we present our data curves and show in qualitative detail that the observed behaviour demonstrates that flux line cutting occurs and associated breathing in and out of nonparallel flux lines takes place across the surface of type II superconductors subjected to a varying $\vec{H}_{ext}$.

Contents

List of Figures

Chapter 1

Introduction

1.1 General Introduction

The discovery of superconductivity in 1911 by Heike Kamerlingh Onnes[25] in mercury cooled below 4.2 K was seen by some as having near limitless prospects in practical applications as well as an avenue towards greater scientific understanding of our physical world. In the decades following, great strides were made in our theoretical understanding of the superconductive state. However the slow progress in raising the critical temperature needed for superconductivity has, until recently, hampered research and limited practical applications (which in turn limited funds available for researchers).

The remarkable discovery in 1986 of the ever increasing family of perovskite superconductors and the rapid increase in T_c from 23K to $\approx$120K, hence above the boiling point of liquid nitrogen, has seen a tremendous surge in the level of research and as well, the number of researchers in the field. This immigration of new personnel from other specialties will most certainly have a great effect on our level of understanding of the superconductive state. The problems posed in gaining a theoretical understanding of the mechanisms required to explain the critical temperatures obtained in

these new High T_c superconductors are to say the least, impressive. Modifications may be made to the existing, phonon mediated, BCS theory or a new view altogether may be needed for this class of superconductors. It is apparent that ideas born out of the great variety of researchers now in the field are needed in the search.

A danger does arise however, in the possibility of new concepts or theories reaching acceptance among the new community of workers without proper awareness of the wealth of information gathered over the decades of research on the low T_c materials.

One of the purposes of our investigations was to provide new evidence in support of an important phenomenon that, unfortunately is not generally known by many new to the field. The phenomenon is that of flux line cutting or the cross flow of non parallel flux lines. Recent experimental[20] and theoretical work[26, 2] is focusing attention on these fascinating processes.

1.2 Review of Flux Dynamics

1.2.1 Collinear Regime

Before proceeding to a discussion of flux line cutting, a brief review of relevant background material is in order. It is well established that certain materials exist, called type II superconductors, in which magnetic flux may be contained within the bulk of the specimen. The flux is seen to exist as quantized vortices or flux lines, each containing a quantum of magnetic flux $\phi_o = h/2e$. Each flux line has associated with it a configuration of magnetic flux density $\vec{B}(\mathrm{r})$ and circulating vortex current density $\vec{j}(\mathrm{r})$. If we imagine two separate parallel flux lines existing in a specimen, the total energy arising from the superposition of these quantities is diminished by increasing their separation. As a consequence, parallel flux lines repel one another.

As a guide to visualization, we invoke the scenario of an infinite slab to describe the effect of an applied external field. With a rising external field $H < H_{c1}$, reversible

Meissner surface currents are generated to shield the bulk of the sample from the field. These currents cannot exist with an infinite current density at the surface so a decaying magnetic field profile arises in the specimen adjacent to the surface with the characteristic length λ, the penetration depth.

As the external field surpasses H_{c1}, flux lines begin to be nucleated at the surface. These are repelled by the exterior field, hence are driven into the interior of the slab where they set up a flux line lattice in equilibrium with their "repulsive" neighbors. The existence of such a flux line lattice was first predicted in great detail, by Abrikosov[1]. This scenario is shown in Fig 1.1(a) and depicts how the magnetic flux density inside the bulk is weaker than the external field.

The above picture does assume that the flux lines are free to move with ease within the sample and describes the ideal or reversible Type II superconductor. Imperfections within the sample may often impede the motion of flux lines. These imperfections can take the form of point defects, vacancies, dislocations, etc. In the vicinity of these imperfections the superconducting state is perturbed, weakened or entirely suppressed. The axis or core of a flux line has to be a normal state region, where the condensation energy of the flux line is sacrificed. If this axis or core overlaps a volume where the material is already normal over lateral dimensions comparable to the coherence length, ξ, then the energy cost is already paid. Thus the flux line is attracted to the imperfection and resists dislodging. In most instances an individual flux line is held in place by a number of such pinning sites. Consequently, as can be readily visualized, a long dislocation of radius corresponding to the coherence length and coinciding with the flux line axis serves as an optimum pinning site. For example, ion track damage in High T_c crystals[9] provide powerful pinning centers for flux lines oriented along their length.

Type II superconductors containing pinning sites are said to be hard, non-ideal or irreversible. Returning now to the infinite slab scenario, the situation is encountered

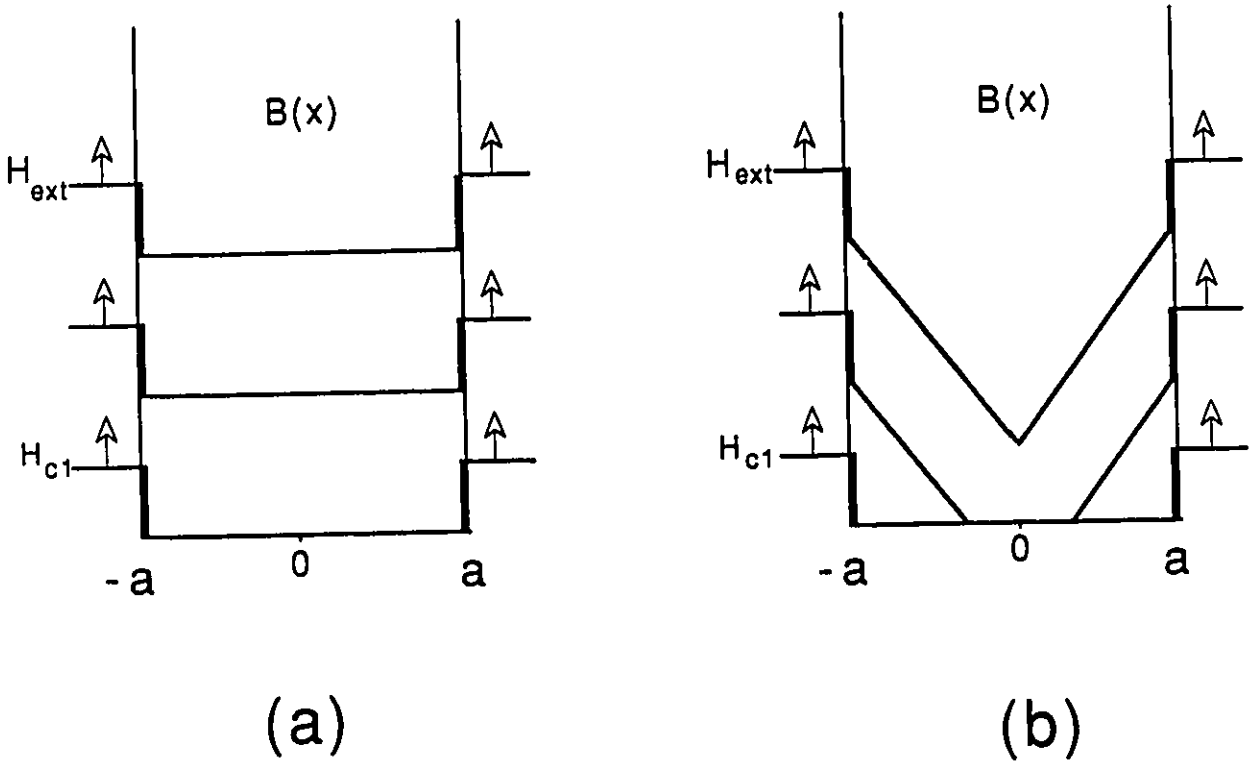

Figure 1.1: Schematic of (a) $B(x)$ profile for an "ideal" or pinning free specimen, (b) $B(x)$ profile for an irreversible specimen containing pinning sites. Surfaces of the infinite slab are situated at $\pm a$.

where newly created flux lines attempt to move inward from the surface but pinning opposes their displacement. Raising of the external field continues to nucleate more and more flux lines. Eventually the pressure of the repulsion exerted by the applied field on the adjacent flux lines becomes great enough to overcome pinning and the flux lines slip forward to new pinning sites. The dynamics of the flux penetration will be further discussed in this thesis. The resulting magnetic flux profile is sketched in Fig 1.1(b). One can readily understand that in these circumstances the average field within the specimen will not keep in step with the exterior field. Hysteresis will therefore be encountered. Increased pinning results in a higher internal field gradient and consequently a larger hysteresis.

1.2.2 Noncollinear Regime

Thus far our discussion has focused on non uniform configurations of parallel flux lines. In these situations, by Maxwell's eqn, $\nabla \times \vec{H} = \vec{j}$, persistent currents flow perpendicular to the magnetic flux density. This situation is sometimes referred to as the collinear regime because here, $\Delta\vec{H}$, each increment (decrement) of $\vec{H}$ is directed along the existing $\vec{H}$. This particular regime has attracted the near exclusive attention of researchers over the years.This is the situation encountered in standard electromagnets, transformers, solenoids, etc.

The term, noncollinear regime is used to describe the more general situation where a component of the current density flows parallel to the field. This regime is denoted noncollinear because here, $\Delta\vec{H}$ an increment (decrement) of $\vec{H}$ is tilted with respect to the existing $\vec{H}$. Under these circumstances, Maxwell's equation, $\nabla \times \vec{H} = \vec{j}$, requires that the orientations of the flux lines vary spatially. Now the interaction of non parallel flux lines must be addressed.

We envisage a succession of sheets of parallel flux lines nucleating at the surface of a specimen bathed in an applied field $\vec{H}$ which is increasing in magnitude and is

also changing orientation. A new sheet of flux lines in this succession will nucleate at a different angle from the previous and will exert a repulsive force upon its predecessors. These may be held back by pinning forces. At this juncture flux cutting processes would serve to relieve magnetic pressure. Either simple cross flow or vortex reconnection followed by a reorientation of adjacent sheets to an intermediate angle could accomplish this. Both of the above scenarios, require that the adjacent sheets of flux lines come into intimate contact. It is well established, however, that parallel flux lines repel each other. Josephson[19] in 1966 and recently others in High T_c work[23, 24] have regarded that the energy needed locally for fusion of flux lines to occur, presents an insurmountable barrier for the flux cutting process. These workers therefore pursued a variety of flux dynamics and contortions to explain experimental results.

Regardless of the arguments and controversy regarding the barrier and local energy, much experimental evidence exists in support of flux line cutting. The basic observation that first led to the concept of flux cutting is the following. A voltage, less than that in the normal state, is measured when a steady current I flowing along a wire surpasses a critical level I_c in the presence of a static externally applied magnetic field directed along the wire[7, 27, 8].

The voltage observed is termed a flux flow voltage and is believed to result from the motion of flux within a sample. Josephson's equation,

$$\vec{E} = -\vec{v} \times \vec{B} \tag{1.1}$$

expresses the relationship between the transport electric field $\vec{E}$, the velocity $\vec{v}$ and the density $\vec{B}$ the of flux lines.

In the absence of an externally applied field (H_a=0), see Fig 1.2 (a), then as the self field increases with increasing current, flux in the form of smoke rings will nucleate at the surface of the wire and be forced to contract inwards by line tension

and the mutual repulsion with new flux rings. This motion will of course be impeded by pinning. A critical current I_c is established when the flux front has just reached the central axis. Any further increase in the current I beyond I_c, nucleates flux rings at the surface which drive the small flux rings, closest the axis, to self annihilation. As each flux ring annihilates at the center the entire flux line configuration migrates inward and new flux lines nucleate at the surface. Thus any steady current above I_c causes a continuous flow of flux lines which gives rise to an electric field,

$$E_z = -v_r(r)B_\phi(r) \tag{1.2}$$

from equation (1.1).

We now consider the situation where a static external field H_a is applied parallel to the length of the wire hence parallel to the current. In these circumstances, the flux lines nucleating at the surface will be helical since $\vec{H}_{total}$ at the surface arises from the superposition of $\vec{H}_a = \hat{z}H_\parallel$ and the self field of the current $\vec{H}_I = \hat{\phi}H_\phi$, (see Fig 1.2 (b)). A critical current I_c is established when the now helical flux line front is driven to the central axis The collapse of helical flux towards the axis destroys its azimuthal component, hence producing an electric field E_z. The longitudinal component however does remain. Hence a paradox results since a steady state voltage at current $I > I_c$, due to flux flow implies a continuous build up of longitudinal flux along the axis. This is clearly impossible.

Flux cutting was brought forth to explain the voltage seen and resolve the problem of accumulation of axial flux [3, 10, 12]. Different detailed models have been proposed involving different scenarios. All involve the continuous counter flow of flux across the surface when I_c is exceeded. For each helical flux line nucleated at the surface, with helicity dictated by the combination of H_ϕ and $H_\parallel$, another flux line is ejected from the sample with a smaller or even opposing helicity. The condition for a steady state is met since for each quantum of longitudinal flux entering the sample, one exits. The

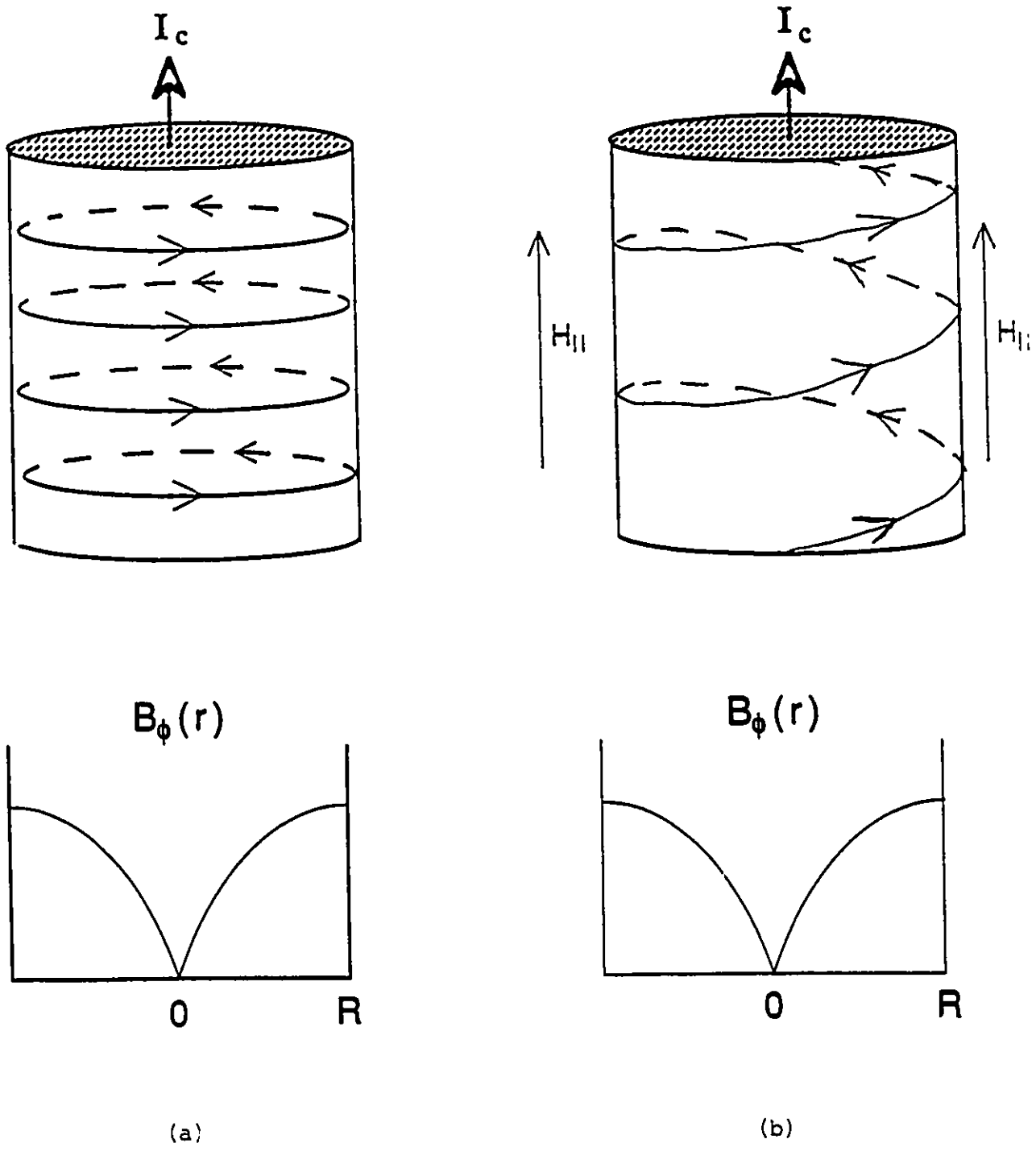

Figure 1.2: (a) The purely azimuthal field and $B(r)$ profile of a current carrying wire at I_c. (b) In the presence of an externally applied magnetic field directed along the wire, flux lines adopt a helical structure

difference in azimuthal component of the entering and exiting flux lines gives rise to the voltage observed. (We shall examine briefly the two common models later in this thesis).

1.3 Merits of Hollow Cylinder Geometry

Over the years, LeBlanc and co-workers have investigated flux line cutting in a variety of materials and for various geometries. For instance they have studied,(i) current carrying wires and ribbons in a longitudinal field $H_{\parallel}$, and (ii) rotating disks in fields parallel to their broad surfaces. Finite geometry because of end effects, hence an appreciable demagnetizing factor, introduces distortions of the magnetic field and problems in the analysis of observations. Ribbons or disks must be made thin to minimize this aspect.

For this and other reasons Fillion[16] and Golebiowski[18] of this lab, adopted long hollow cylinder geometry where the demagnetizing factor along the azimuthal direction disappears. More importantly however are the unique possibilities brought forth in the use of this geometry. The hollow center of a superconducting cylinder provides an isolated environment in the sense that once cooled below T_c, the magnitude of longitudinal flux can then only be altered by flux arriving from, or exiting to, the wall of the cylinder. Thus a reservoir of flux is created whose content can be monitored easily and can be influenced by processes occurring in the wall of the sample as a result of varying applied fields.

Depending on the experimentalists goals a set up employing hollow cylinder geometry would include the following. (i) A toroidal magnet coil giving control of the azimuthal field H_{ϕ} applied on the inner and outer surface of the hollow cylinder. (ii) An outer solenoid fixing the boundary condition of the axial field $H_{\parallel}$ on the outer surface. However, the level of axial magnetic flux density in the hole (B_{zh}) is not

in direct control of the experimentalist. (*iii*) Inner and outer axial pick up coils, the former registering the level of axial flux in the reservoir and the latter providing data on the average longitudinal flux density $<B_z>$ permeating the sample wall. (*iv*) A toroidal pick up coil wound through the hole and around the wall of the hollow cylinder gives the average flux density $<B_\phi>$ in the wall.

Fillion in his research for his Ph.D thesis employed all of the above and was able to study a rich variety of phenomenon with much success. In later work Golebiowski improved on the arrangement and in the course of his work, fascinating behavior was observed that shed light on the flux cutting process. The hollow cylinder under study was fabricated using a $PbBi$ alloy with a high H_{c2}. Due to limitations in the available toroidal magnetic field, H_ϕ, he was not able to fully witness an interesting phenomenon reported in this thesis. In our work, this phenomenon was made to emerge in its entirety. This success was obtained by preparing a sample with a lower H_{c2} accessible to our superconducting magnets and by endeavoring to maximize H_ϕ. In order to accurately monitor the evolution of $B_{z\,hole}$, the crucial piece of information on the behavior under study, it is important that the area/turn number of the inner pickup coil be maximized. To accomplish this and make more area available for this coil we elected to omit a toroidal pickup coil. Although it is desirable, for completeness, to monitor $< B_\phi >$ simultaneously with $B_{z\,hole}$ and $B_{z\,wall}$ the behavior of $< B_\phi >$ is already quantitatively well established under the circumstances under scrutiny and its detailed performance plays no role in the interpretation.

Chapter 2

Experimental Set Up

2.1 Choice of Sample

The choice of hollow cylinder geometry leads to some rather important design restrictions. On the one hand a large inner diameter would facilitate a healthy inner pick up coil and also more numerous windings of the toroidal magnet coil. To counter this, a larger inner area would result in a larger internal reservoir of axial flux. With such a large reservoir, monitoring the change of its level as small amounts of axial flux are drawn into or expelled from the walls of the sample, would require increased sensitivity.

Also within the goal of minimizing sample dimensions, the fact must be faced that large fields will not be obtained with the toroidal magnet. We thus required a sample with a modest upper critical field H_{c2} which could be reached by the vectorial combination of the azimuthal field of the toroidal magnet coil and axial field of the solenoid.

A suitable candidate was found in a $PbIn$ alloy in particular $Pb_{0.85}In_{0.15}$. From a literature search and past laboratory experience, $PbIn$ was found to have many desirable characteristics. It met the criterion of a modest $H_{C2} \approx 2000$ Gauss at 4.2

K and its superconductive transition temperature is around 6 K, hence studies could be conveniently performed in liquid helium boiling at one atmosphere thus bypassing the need to pump on the helium. Also the low melting points of the constituents makes preparation of large ingots a relatively straight forward matter. It should also be mentioned that these metals are inexpensive.

An ingot was prepared by mixing cuttings of high purity Pb and In in the desired proportions. This mixture was melted in a sealed, evacuated quartz glass tube at a temperature of $\approx$ 500 °C. The tube was then periodically shaken at this temperature over a number of hours, followed by cooling gradually to room temperature by switching off the oven.

It is known that the pinning characteristics of the $PbIn$ alloy can be greatly affected by its preparation technique[21]. For instance, rapid quenching from the melt can lead to high pinning or conversely a modest annealing process will remove pinning sites from the ingot. In our specific study the role of pinning is not of immediate interest hence the detailed ingot fabrication process is not pertinent.

From the cylindrical ingot, a hollow cylinder of length 60 mm, inner radius 7 mm and outer radius 10 mm was prepared by machining on a lathe and then having the inner cavity bored out. No chemical treatment or mechanical cold work was performed on the cylinder to affect its properties.

2.2 Experimental Set Up

2.2.1 Sample Heater Assembly

The exact temperature of the sample is neither strictly controlled nor monitored in the course of the experiments. Maintaining T at the ambient temperature of 4.2 K of the helium bath is sufficient. It is however necessary to be able to raise the temperature of the entire sample above T_C. This is crucial, since to correctly determine the behavior

of a real, hence hysteretic, type II superconductor, the initial configuration of the magnetic flux must be specified. Consequently, before a measurement is undertaken, the slate must be wiped clean, ie. any previous magnetic field history must be erased by raising the sample above T_C to the normal state.

We then ensure that the transition to the superconducting state occurs in the desired stationary applied fields H_ϕ and $H_\parallel$. This procedure is referred to as Field Cooling. The inevitable close proximity of the toroidal magnet winding (see Fig 2.1) and the heating coil introduces some problems and limitations. The temperature of the sample must be brought above T_c without also driving the current carrying $NbTi$ wire of the toroidal magnet normal.

Heating of the hollow cylinder is accomplished by driving a steady current through a manganin 38 gauge wire wound non-inductively (ie. bifilarly) in intimate contact with the outer surface of the cylinder. The good thermal conduction of the sample ensures that a modest surface heating drives the entire bulk into the normal state. Unwanted heating of the nearby toroidal magnet winding is reduced by a layered thermal barrier of packing tape covering the sample and heater coil layer. Manganin wire is ideal for the heater coil since it is non magnetic and has a large and reasonably temperature invariant resistance. The large resistance allows the required joule heating to be achieved with low currents (milliamp range). Any magnetic fields generated by the heater are thus minimized both by the noninductive windings and the use of small currents.

Two delrin end caps, providing small shoulders facilitated the winding of the heater coil and ensured that the single layer of heater coil extended to the extremes of the cylinder. These fixed end caps also provided a firm structure for the toroidal windings to follow.

2.2.2 The H_z and H_ϕ Magnets

Our investigations entailed varying the azimuthal component of the magnetic field using a toroidal coil whilst maintaining a steady axial field with a standard solenoid arrangement.

Our choice of a $PbIn$ alloy sample with modest H_{C2} means that the fields required of the solenoid and toroidal magnet coil are not excessive. The generation of the desired axial component is a fairly straight forward matter. A solenoid was constructed to completely surround and bathe all other components in an axial field. Its length was made appreciably longer than the hollow cylinder sample to minimize end effects. The solenoid dimensions are; length 16.3 cm, inner radius 2.1 cm, outer radius 2.6 cm. It comprises 2965 turns of $NbTi$ wire and provides a field of 0.0217 $Tesla/amp$ thus generates adequate axial fields using a modest 10 amp ripple free DC power supply.

The construction of a toroidal magnet which could provide the required azimuthal fields presents a serious obstacle. In previous studies, Fillion and Golebiowski were capable of reaching high azimuthal fields with a small number of toroidal turns (7 and 16 respectively). This was possible due to the fact that larger gauge, multifilamentary $NbTi$ wire was utilized which could sustain the full 400 amp current possible with battery bank driven power supply in our laboratory. It was desired to operate at the more moderate 100 amp range to limit joule heating of the copper leads and for other concerns. As a result, many more turns were necessary for the toroidal coil. After the insertion of an inner pick up coil system (see next section) there remains an inner diameter of 5mm in which to pass the turns of the toroid. Using smaller gauge $NbTi$ core wire of 0.4 mm diameter, 62 turns were obtained in the available space.

Using Ampere's Law;

$$\oint \vec{B} \cdot \vec{dl} = \mu_o I \tag{2.1}$$

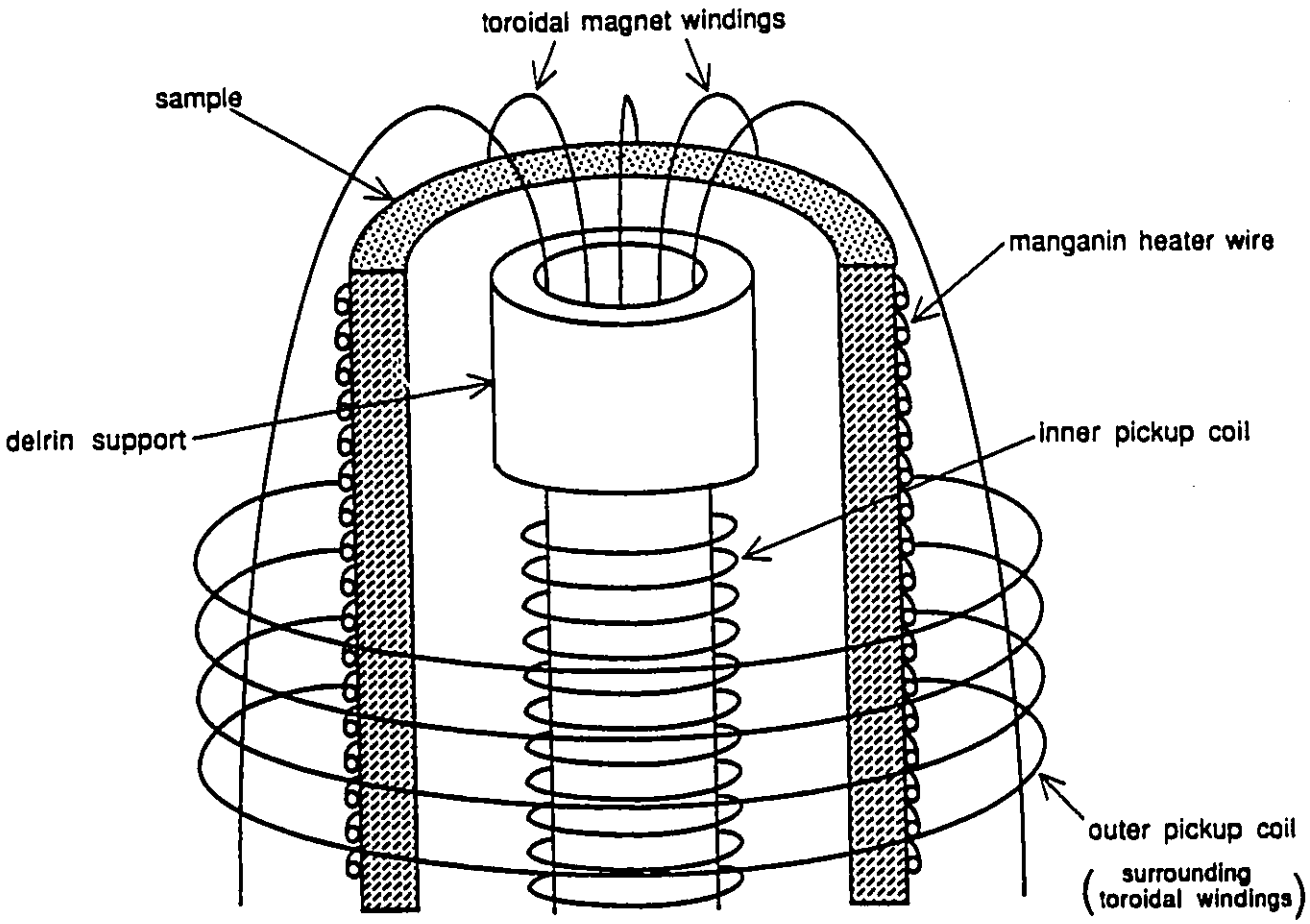

Figure 2.1: Schematic of apparatus contained within outer solenoid magnet

we can express the azimuthal magnetic field in the space embraced by the toroidal windings as;

$$B_\phi = \frac{\mu_o n I}{2\pi r} \tag{2.2}$$

where n is the number of turns, r the radius and I is the current carried by each turn. It is thus noted that due to the finite thickness of the sample walls, the azimuthal flux density along the inner surface is greater than that at the outer surface and their ratio reads,

$$\frac{B_\phi(R_o)}{B_\phi(R_i)} = \frac{R_o}{R_i} = 1.4 \tag{2.3}$$

where R_o and R_i are the outer and inner radius respectively.

The average azimuthal magnetic induction permeating the wall of the cylinder in the normal state, is given by,

$$< B_\phi >_{applied} = \frac{\int_{R_i}^{R_o} B_\phi(r)dr}{\int_{R_i}^{R_o} dr} = \frac{\mu_o n I}{2\pi(R_o - R_i)} ln(\frac{R_o}{R_i}) \tag{2.4}$$

The connection between the ends of the superconducting toroidal magnet wire and the copper leads extending to the power supply is another delicate matter. Resistive contact heating, if not minimized and rapidly transferred to the helium bath could raise the temperature of the adjacent superconducting wire above T_c, thus destroying its high current carrying capacity. To reduce the contact resistance the ends of the toroidal magnet winding were sandwiched between thin sheets of indium and pressed tightly between massive copper blocks. The soft indium ensures intimate contact by wetting the $NbTi$ wire as well as the copper blocks thus reducing the contact resistance and heating. The large volume of the copper blocks provides both a large heat sink and good heat transfer to the helium bath. Large copper leads attached to brass screws in the copper blocks bring the current from the power supply.

Further precautions must be taken to protect the toroidal magnet winding from damage (local melting) under high current operation where the critical current I_c is reached in the weakest segments. In such an event, the 0.075 cm thick copper

sheath frequently provides insufficient protection. Consequently an electronic system was used to automatically shut down the current supply within a few milliseconds of the onset of a superconducting to normal transition. The transition is sensed by the development of an appreciable voltage drop across the toroidal magnet coil. With these safety precautions operating reliably we can comfortably raise the current in the toroidal magnet until I_c is attained and it transits to the normal state. This sets an upper limit on the azimuthal field we can obtain. In our arrangement we achieved steady azimuthal fields up to $\approx$ 0.15 Tesla with a current of $\approx$ 100 A. This proved quite adequate for our investigations.

2.2.3 Pick Up Coil and Monitoring System

It is of course desirable to monitor the magnetic flux density in both the azimuthal and longitudinal orientations. To accomplish this for the azimuthal direction entails hand winding a toroidal pick up coil of a few thousand turns through the hollow cylinder and along its outer surface. The detailed evolution of the azimuthal magnetic flux density is however of no importance in our specific investigation. Also, the space taken up by these windings would lead to a diminution in the strength of the toroidal magnet and lower the sensitivity of the pivotal inner longitudinal pick up coil and thus jeopardize the overall success of our endeavor. The evolution of the azimuthal flux in these materials is "classical" and has been well documented by Fillion and Golebiowski. It was thus decided to omit the toroidal pick up coil in this pioneering study. It is also worth noting that complementary follow up studies are underway in our laboratory where the evolution of the azimuthal flux density will be monitored on a sample identical to ours in composition.

Two azimuthally wound pickup coils sense the component of magnetic flux density along the z direction. One coil is placed inside the hollow cylinder and monitors, B_{zhole}, the "level" of longitudinal flux density in the cavity or reservoir. The other is

wound around the waist of the cylindrical sample and simultaneously monitors the average flux density permeating the wall of the cylinder and the cavity. The average flux density permeating only the wall, $< B_z >_{wall}$, can be obtained using these two signals and the definition of magnetic flux ϕ and the corresponding averages. Thus,

$$\phi_{total} = \phi_{wall} + \phi_{hole} \tag{2.5}$$

hence,

$$< B_z >_{total} \pi R_o^2 = < B_z >_{wall} \pi [R_0^2 - R_i^2] + B_{z\,hole} \pi R_i^2 \tag{2.6}$$

Rewriting

$$< B_z >_{wall} = < B_z >_{total} \frac{R_o^2}{R_o^2 - R_i^2} - B_{z\,hole} \frac{R_i^2}{R_o^2 - R_i^2} \tag{2.7}$$

Thus $< B_z >_{wall}$ can be found by subtracting the signal of the inner pickup coil from the outer pickup coil signal either electronically or digitally.

The inner pick up coil is wound inside a delrin spool that fits snugly into the hollow cylinder. This maximizes the area enclosed by this coil. It is hollow to allow space through which the toroidal magnet coil is threaded and wound. The coil is comprised of about 16,000 turn of 42 gauge formvar insulated copper wire and has an inner diameter of 3mm and outer diameter of 6mm. It is centered along the middle of the cylindrical sample and its length is deliberately made appreciably shorter than the sample to minimize detecting end effects.

The outer pick up coil embraces the entire set up of sample, toroidal magnet and inner pick up coil. Again its length is about half that of the sample and is centered to monitor the waist of the sample. It consists of around 30,000 turns with an inner radius of 1.51 cm and an outer radius of 1.80 cm. It is balanced by two bucking coils so that any flux density change due to changes in the applied field $H_{\|}$ are negated. The two bucking coils carry about 18,000 turns each wound oppositely to the main pick up coil. The slightly higher area-turn product needed reflects the slightly lower flux density found nearer the ends of the outer solenoid.

The output from each pick up coil is fed into an integrating amplifier (PAR Model 215) each of which in turn drives the Y-axis of an $X - Y$ recorder. In our work the longitudinal applied field is kept fixed while the azimuthal field is varied. The X axis of each recorder is connected to a shunt monitoring the current flow through the toroidal magnet coil. Thus the two signals are monitored simultaneously as the toroidal field H_ϕ is varied.

2.2.4 Calibration

The phenomenon of near perfect shielding of a virgin sample against a weak magnetic field $H < H_{C1}$ is made use of to calibrate the readings from the outer pick up coil. Below H_{c1} the shielding currents flow in a penetration depth λ at the surface of the superconducting hollow cylinder experiencing the applied field. As λ is minute compared to the dimensions of the sample, perfect diamagnetism is an excellent approximation. A virgin sample signifies that the sample has been lowered through T_c in zero field. Thus in this regime of low fields, the integrated signal from the outer pickup coil and registered on the Y axis will be directly proportional to the axial magnetic moment of the hollow cylinder. Because of perfect shielding the latter is proportional to the applied field $H_\parallel$.

The inner pickup coil is calibrated by monitoring its response to a known change in $H_\parallel$ with the hollow cylinder maintained in the normal state just above T_c by means of the manganin wire heater.

For each cycle of H_ϕ with $H_\parallel$ being held fixed, the measurement is repeated with the sample kept normal by heating to above T_C. This provides a reference or background curve which measures the contribution to the signal arising from the fact that the pick up coil and bucking coil are not perfectly balanced.

One final point on the acquisition of data bears mentioning. This arises from complex patterns of circulating persistent currents in the coil windings induced by

the changes of H, caused by and experienced by the windings.As a consequence $H(I)$ function of superconducting magnet coils is not linear or reversible but exhibits some hysteresis hence history dependence.

This hysteresis, although not serious in our experimental set up, nevertheless needs to be carefully taken into account. In order to obtain reproducible, hence reliable, data and identify this hysteretic contribution to the observed signals, it is important that the sequence and magnitudes pertaining to any cycle of the applied field(s) for a chosen measurement be clearly defined and traversed a few times before the response of the sample to the chosen procedure is monitored.

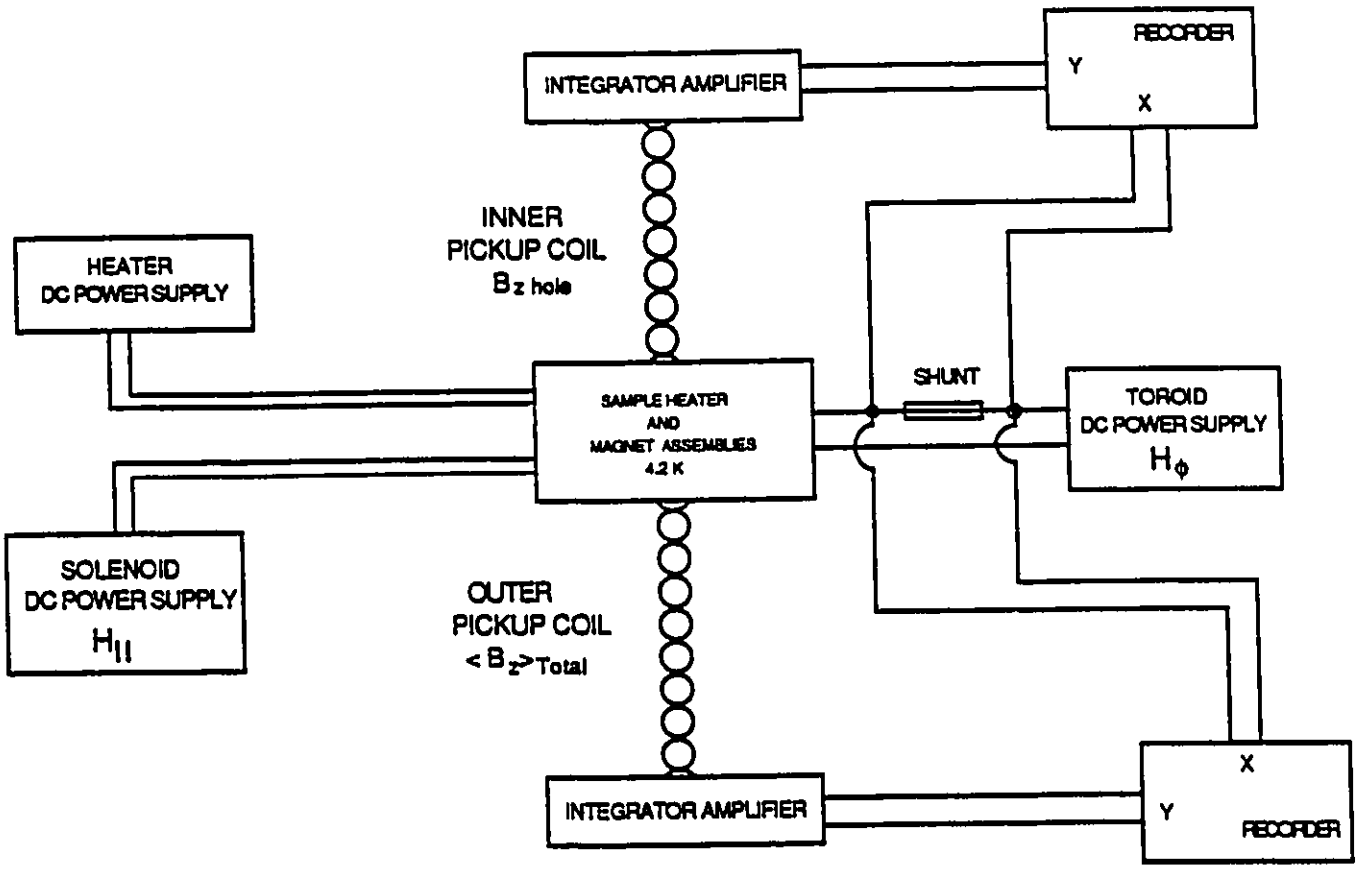

Figure 2.2: Schematic of experimental set up

Chapter 3

Theoretical Foundations

3.1 Introduction

Prior to a discussion of our experimental results an outline of relevant background need be addressed. The background we review is in some sense dictated by the results themselves. We claim that the behavior we observed in our work, supports the concept of flux line cutting and the cross flow of flux line lattices in an exceptionally simple manner. Detailed calculations of the dynamics of the evolution of the $\vec{E}(r)$ and $\vec{B}(r)$ fields are in progress and will be reported in another thesis. This quantitative analysis requires the application of Clem's phenomenological model to cylindrical geometry and is beyond the scope of this masters thesis. We will confine ourselves to a description of the essential features of this framework.

In the following discussion we shall focus qualitatively upon the dynamics and the spatial arrangements of the flux lines within a specimen. A knowledge of the resulting configuration of the flux line density can then be related to the patterns of persistent or transport currents by Maxwell's equation $\nabla \times \vec{B} = \mu_o \vec{j}$

3.2 Critical State

The concept of the Critical State is more readily understood in the collinear regime. It is again simpler to consider infinite slab geometry where the only finite dimension is the thickness along $\hat{x}$. An increasing H_{ext} parallel to the slab will begin to nucleate flux lines at the surface when H_{c1} is surpassed. The migration of these flux lines towards the interior will be impeded if pinning sites exist. It is readily pictured that a nonuniform flux line density profile $B(x)$ will result from the 'pile up' of flux lines.

The $B(x)$ profile will be complicated over the microscopic range of individual flux lines which consist of normal cores surrounded by spatially varying persistent currents. On a quasi macroscopic scale encompassing the cross section of several flux lines, a local current density can be described through Maxwell's equation $\nabla \times \vec{B} = \mu_o \vec{j}$, where the current $\vec{j}$ originates from the superposition of persistent currents circling several individual flux lines. In planar geometry this reads;

$$-\frac{dB}{dx} = \mu_o j_\perp \tag{3.1}$$

In nonideal type II superconductors two competing forces exist. The Lorentz like driving force $\vec{F}_L = \vec{j} \times \vec{B}$ and the pinning force density $\vec{F}_p$ also averaged over the cross section of several flux lines.

The essence of the concept of the critical state is that no flux motion will occur unless F_L exceeds F_p. Thus in planar geometry when flux lines are introduced or removed from a specimen, the flux line density profile $B(x)$ will be dictated by the critical gradient, $dB/dx = \mu_o j_{c\perp}$. Equivalently then, $j_\perp = j_{c\perp}$ wherever $j_\perp \neq 0$. We note that F_p and consequently $j_{c\perp}$ can be a function of both B and T. A complete profile of $B(x)$ can be determined once $F_p(B,T)$ or $j_{c\perp}(B,T)$ is known along with H_{ext} and the sample history in the superconducting state. This prescription allows calculation of the space average of the internal magnetic flux density, $< B(x) >$. Figure 3.1 details pictorially the sequence of profiles of $B(x)$ generated during a half

wave cycle of an external field. Fig 3.1(a) and (b) display $B(x)$ for the simple 'Bean' model where the pinning force F_p depends linearly on the local magnetic flux density B (thus $j_{c\perp}$ is uniform and the slope of the linear B(x) profile is constant). Fig 3.1(c) and (d) represent $B(x)$ where F_p is independent of B. This is referred to as the simple 'Kim' model.

The $B(x)$ profile follows the critical state such that any further change in H_{ext} will result in a flow of flux lines until a new critical $B(x)$ profile is reached. The electric field generated by the changes in the $B(x)$ profiles can be calculated using Maxwell's equations,

$$\nabla \times \vec{E} = -\frac{\partial \vec{B}}{\partial t} \tag{3.2}$$

The critical state has been extensively applied to an analysis of a variety of situations, such as, (i) calculations of the critical current I_c vs H externally applied transverse to I for ribbons and wires and, (ii) low frequency A.C. (hysteresis) losses. In the latter case $< B(x) >$ versus H_{ext} is determined analytically or numerically. These results are then introduced in the standard formula,

$$W = -\oint < B > dH_{ext} = \oint H_{ext}\, d < B > \tag{3.3}$$

for energy dissipation per cycle per unit volume which follows from integrating the Poynting vector over the surface of the specimen and through a cycle of H_{ext}.

3.3 Double Critical State and Flux Line Cutting

To examine the interaction of non parallel flux lines, we again return to the infinite slab (planar) geometry. While the present work has exploited hollow cylinder geometry, the underlying concepts are most readily conveyed in this simpler geometry.

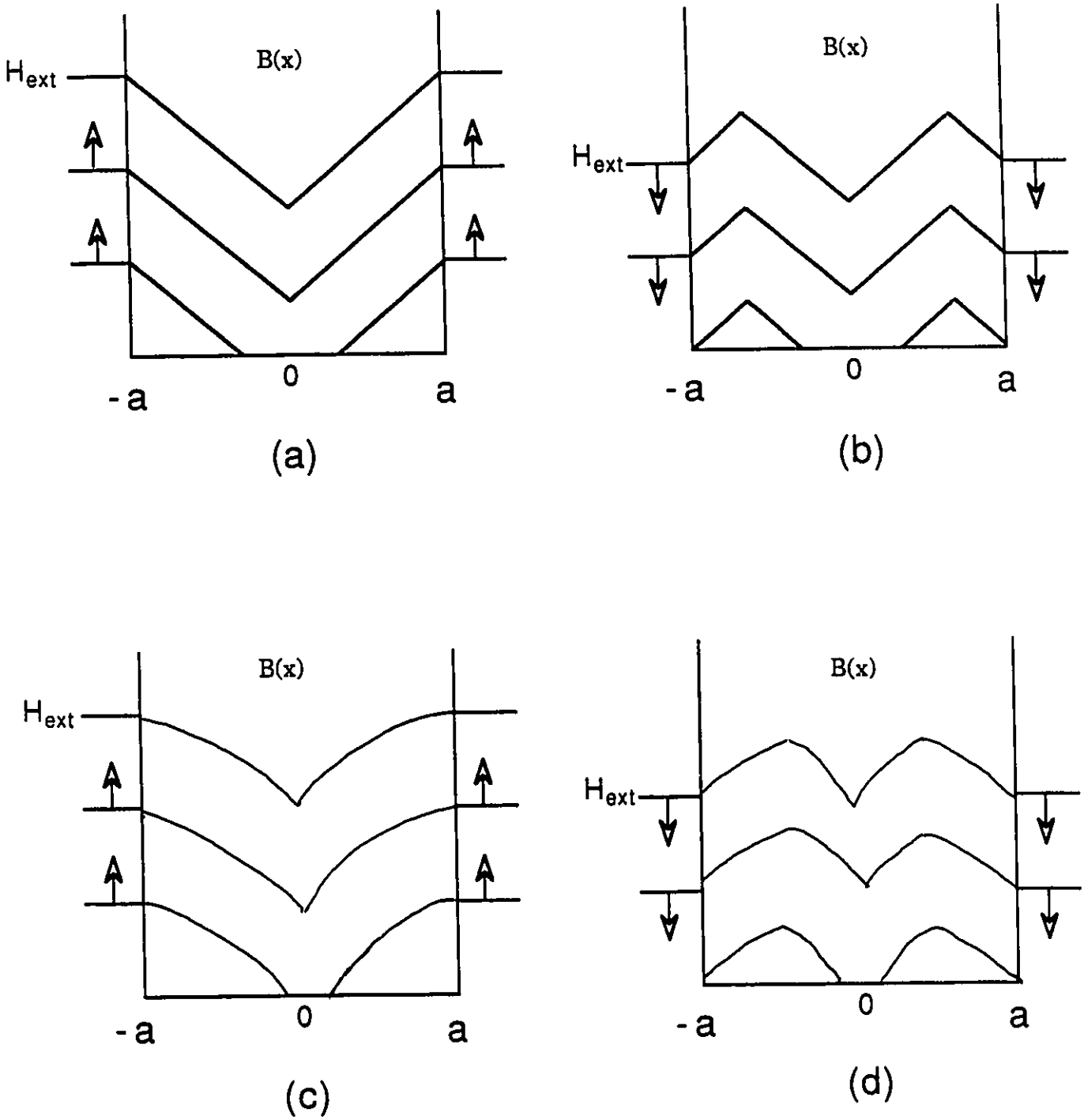

Figure 3.1: (a,b) Half wave cycling and resultant $B(x)$ profile for "Bean" model $dB/dx = \mu_o j_{c\perp}$ where $j_{c\perp}$ is a constant. (c,d) for "Kim" model $dB/dx = \mu_o j_{c\perp}(B) = \alpha/B$. The sufaces of the slab are located at $\pm a$.

It is useful to first examine the dynamics of flux lines in a simple scenario under the assumption that flux line cutting is energetically unfavored and does not occur. In this scenario $\vec{H}_{ext}$ is simultaneously increasing in magnitude and changing orientation. Fig 3.2 depicts the situation after the slab has cooled below T_c in a steady longitudinal field $H_\parallel$ (this process is referred to as Field Cooling, FC). If Meissner currents are ignored, for simplicity, then the flux line density, $B_\parallel$, within the slab will be uniform and equal to the externally applied magnetic flux density.

The application of a complementary field perpendicular to the original longitudinal field and also parallel to the surface will result in a total exterior field;

$$\vec{H}_{ext} = \vec{H}_\parallel + \vec{H}_\perp \tag{3.4}$$

The flux line density gradient will govern the critical profile. Thus as displayed in fig 3.2(a), all of the original longitudinal flux lines will be compressed in a now smaller volume extending from $-x_i$ to $+x_i$. Consequently, each new flux line nucleated at the surface due to the increase of $\vec{H}_\perp$ will add one quantum of flux to that already permeating the slab longitudinally.

The angle profile, $\theta(x)$, the direction of the magnetic flux density $B(x)$ in the y-z plane as a function of depth x, is dictated solely by conservation of flux when no flux cutting takes place. Also it is readily noted that $-x_i$ and x_i, the fronts of the angle disturbance, mark the outer volume boundaries of all the original longitudinal flux lines.

Clearly then, the constraint that flux lines do not cut leads to the conclusion that a monotonic increase in the $< B_\parallel >$ component should be observed. However it is frequently observed that this component diminishes upon the increase of $\vec{H}_{ext} = \vec{H}_\parallel + \vec{H}_\perp$ by increasing $H_\perp$ with $H_\parallel$ fixed.

To account for these results it is frequently naively proposed that torsional forces can cause the flux lines to rotate in the direction of $\vec{H}_{ext}$, thus diminishing the $< B_\parallel >$

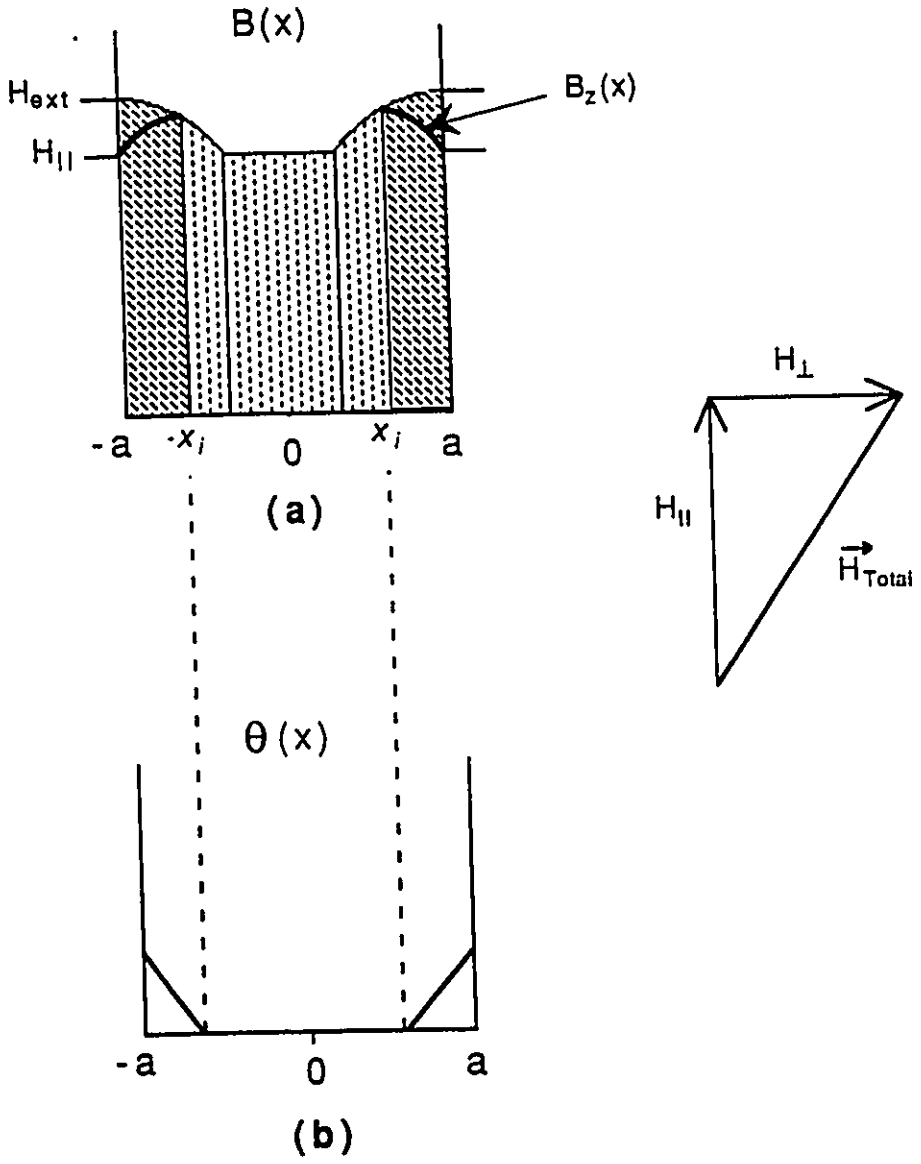

Figure 3.2: (a) $B(x)$ profile for infinite slab, vertically thatched area represents the volume containing all the original flux at time of cooling. (b) The corresponding angle profile $\theta(x)$. The angular disturbance has penetrated to $\pm x_i$

component. A careful examination of the magnitude of the torque or torsional forces which come into play shows that this explanation is inadequate. We now summarize the argument.

Adjacent sheets of non parallel flux lines cannot exert a torque on each other by their interaction within the volume of the specimen. This absence of a torque is a consequence of the fact that the Lorentz force $\vec{F}_L = \vec{j} \times \vec{B}$ is directed perpendicularly to the sheets. Any torque which appears must originate from the forces acting on the ends of the flux lines where they pierce the surfaces of the specimen. The effective volume of action of these forces is then $\approx \lambda d^2$, where λ is the penetration depth and d^2 is the "cross section" of the flux line. However, the pinning and viscous forces restraining the rotation of the flux line extend over a volume Ld^2 where L the length of the flux line stretches along the entire sample, hence $L >> \lambda$.

Brandt et al[3] investigated the activation energy and interaction forces between two straight flux lines as a function of their separation and the angle θ subtended by their axis. They showed that the activation energy was finite even in the London limit of vanishing normal core radius. Josephson[19] in an earlier paper had examined various scenarios of entangled flux lines unable to cross each other since he regarded the energy barrier for flux cutting as too large to permit this process to occur. Brandt et al[3] also examined the interaction of two tilted straight flux lines in the context of the Ginzberg Landau theory exploiting an analytic approximation for the core region. Now two competing interactions come into play. An attractive interaction now originates from the lowering of the free energy due to the overlap of the normal cores of the two flux lines. They found that this attractive interaction could dominate the electromagnetic repulsion and lead to an overall attraction when the angle between the two lines was less than 90^0. Further they found that the attraction increased as the Ginzberg-Landau parameter κ decreased from large values. They concluded that flux line cutting was probable in low κ materials.

Clem and Yeh[12] pursued this analysis and considered the interaction of a flux line lattice consisting of equally spaced sheets of vortices where the vortices in each plane or sheet are parallel to each other but a difference of angle $\Delta\theta$ exists in the direction of adjacent parallel sheets. This investigation confirmed that when $\Delta\theta$ was larger that a critical value $\Delta\theta_c$, the adjacent sheets of flux lines experienced a net attraction, hence could undergo flux line cutting. We note that, in the fundamental framework of Maxwell's equation $\nabla \times \vec{B} = \mu_0 \vec{j}$, a critical angle gradient $(\Delta\theta/\Delta x)_c$ implies a critical current density $j_{c\parallel}$, flowing parallel to the sheets of flux lines and giving rise to their different orientations.

Prior to these theoretical developments LeBlanc and his co-workers had, on empirical grounds, introduced a Double Critical State Model. This model assumed that, in the noncollinear regime, any change in flux line orientation within a specimen would follow a critical angle gradient $(d\theta/dx)_c$. This idea of a critical angle orientation gradient was added to the well established Critical state concept that flux lines could migrate and a flux line density gradient arise only when the current density $j_\perp$ perpendicular to the flux line density exceeded a critical value $j_{c\perp}$.

Consequently, in the framework of Maxwell's equation, $\nabla \times \vec{B} = \mu_o \vec{j}$, these two critical state assumptions for planar geometry read,

$$-\frac{dB}{dx} = \mu_o j_{c\perp}(B) \tag{3.5}$$

$$B\frac{d\theta}{dx} = \mu_o j_{c\parallel}(B) \tag{3.6}$$

Exploiting these simple formulae, LeBlanc and collaborators described with success a wide variety of experimental results.

LeBlanc and his collaborators recognized that in regions where the density of non parallel sheets of flux lines was undergoing decompression, the initial angular orientation profile $\theta(x)$ would correspondingly stretch out. Consequently in these

expansion zones $d\theta/dx$ would drop below $(d\theta/dx)_c$ hence $j_\parallel$ becomes less than $j_{c\parallel}$. The conditions for the appearance of such zones and their boundaries could readily be identified and treated consistently by applying the laws of electrodynamics. In these regions, flux line cutting does not occur and this process is not required in the account of the evolution of the $\theta(x)$ profile in these zones as their boundaries advance or retreat.

The new assumptions, although useful and successful in accounting for a multitude of observations are however too far reaching. Other situations besides the decompression regions already mentioned above, can be envisaged where $j_\parallel$ can exist at a value less than $j_{c\parallel}$, hence $(d\theta/dx)$ remains below $(d\theta/dx)_c$, in the noncollinear regime. Specifically we must consider the situations where the changes in the magnitude of $\vec{H}_{ext}$ are large but the corresponding variation in its direction, although not zero, are small. For instance, if $\vec{H}_{ext}$ is increasing in magnitude while undergoing a very small angular change, the new flux lines nucleated by the rise in $|\vec{H}_{ext}|$ will possess only a minute angle difference with respect to their predecessors in the vicinity of the surface.

In these circumstances, a lattice of flux lines will be generated in a sub critical state with respect to $(d\theta/dx)$, hence with $j_\parallel < j_{c\parallel}$ but critical with respect to the density gradient dB/dx, hence with $j_\perp \leq j_{c\perp}$. In their approach, LeBlanc and collaborators were compelled to treat these situations separately. Here they applied the principle of conservation of total flux and of the components of the magnetic flux density as these regions expanded and migrated. We note that the $\theta(x)$ profile of the flux lines in these zones subsequently becomes critical as the flux lines are driven into the sample and become compressed against the initial flux lines during their advance into the specimen. This can be seen by noting from eqn 3.6 that $j_\parallel$ will rise as B is made to increase and concurrently, Δx, the separation between the flux lines sheets is diminished. Clem's[11, 14] phenomenological Generalized Critical State Model,

which we will outline later, addressed all of these situations in a grand, self-consistent and unified scheme. Further, Clem's model predicted the occurrence of a new type of region, not previously envisaged where the magnetic flux density could be made to diminish by flux line cutting alone.

Various quasi-macroscopic dynamical models of the flux line cutting process have been proposed (Clem[12, 13, 14], Brandt[4, 5, 6]). We outline the sequence of events envisaged to occur in the simple "single" flux line cutting model. This picture is also referred to as the "Breathing Mode" model when applied to steady state situations. Again, for simplicity, we focus on infinite slab (planar) geometry. We consider two adjacent sheets of flux lines subtending an angle $\Delta\theta > \Delta\theta_c$. Fig 3.3 a,b,c depicts this situation with 3.3(a) taken to be above the plane of the page and 3.3(b) to be just below. It is useful to visualize that the sheet of flux lines of Fig 3.3(a) has been nucleated by an increment in the magnitude of $\vec{H}_{ext}$ accompanied by a significant change in orientation, hence a rise $\Delta H_\perp$ with $H_\parallel$ fixed, sufficient to ensure that $\Delta\theta > \Delta\theta_c$.

Since the angle between the two sheets is supercritical, these attract, hence move closer together (see Fig 3.3(c)) and establish contact with each other forming the array displayed in Fig 3.3(d). At the points of contact of Fig 3.3(d), the fused flux lines form doubly quantized regions which are energetically expensive, therefore unstable. The energy is lowered by a cross joining of the adjacent segments of the original flux lines. The break up of the fused configuration of Fig 3.3(d) is sketched is Fig 3.3(e) and the cross joined adjacent segments in Fig 3.3(f) present a zig-zag pattern. This zig-zag pattern contains considerable line tension energy which is lowered as the flux lines straighten out hence shorten. Fig 3.3(g) depicts the resulting very dense sheet of flux lines lying in the plane of the page after the straightening out of the zig-zag lines has taken place.

This densely packed sheet now has volume available to redistribute itself. Because

of the mutual repulsion of parallel flux lines, the dense sheet separates into the two sheets depicted in Fig 3.3(h) and (i), where one is lying below the page and the other sheet is above the page. Simple geometric construction shows that, D_f, the final separation of the flux lines in each sheet is larger than their initial separation D_i, ie.;

$$D_f = \frac{D_i}{cos(\Delta\theta/2)} \tag{3.7}$$

Since the flux line density B can be written,

$$B = n\phi_o = \frac{\phi_o}{D^2} \tag{3.8}$$

where n is the number of flux lines per unit area, ϕ_o is the quantum of flux, it follows that the process just described leads to a diminution of flux density although the number of flux lines is conserved. This lowering of flux density is a result of the flux line straightening and therefore of the flux line shortening process (see Figs 3.3 (f) and (g)). This process accounts for the decrease of magnetic flux density occurring in zones where only flux cutting is taking place.

Now we visualize that below the paper and adjacent to the two sheets or planes of flux lines whose interaction we have just examined, there initially existed a series of sheets of flux lines to a depth x_i which subtended an angle $\Delta\theta_c$ with respect to their immediate neighbours. Clearly then, after the process which has just been described, $\Delta\theta$ between the sheet labeled (i) in Fig 3.3 and its nearest "interior" neighbour now exceeds $\Delta\theta_c$. Hence, these sheets will now attract each other and undergo the same cutting process just outlined. In this manner, we can see that a "clockwise" reorientation of the entire critical flux line lattice will propagate inwards until a region is encountered where the sheets are parallel, thus $\Delta\theta = 0$. The advance of the disturbance in the orientation of the sheets will then cease after reorienting the uppermost sheet in the collinear lattice. Consequently, the depth of the nonparallel (tilted) sheets will have expanded into the domain of parallel sheets. Thus the front

of the $\theta(x)$ profile will have advanced inward from x_i to $x_f = x_i + \Delta x$ causing one more sheet of the originally parallel flux line region to adopt a tilted orientation.

The advance of the angular disturbance will be accompanied by the penetration of a compression or density disturbance. This arises because we stipulated that at the outset of the events displayed in Fig 3.3, the flux line sheet labeled (a) was nucleated and squeezed into the volume originally occupied only by the sheet labeled (b). We note that the depth of penetration of the density and angular disturbances will generally not be identical.

Also we note that sheets (h) and (i) may find relief from their "squeezed" predicament if the sheet adjacent to the surface is released (expelled) from the specimen. This corresponds to the "breathing" out phase of the breathing mode. The entry (nucleation) of flux lines constitutes the breathing in part of this analogy. Whether the sheet adjacent to the surface is expelled or not, the new sheet which enters the specimen will subtend an angle $\Delta\theta > \Delta\theta_c$ with respect to the immediate neighbour. This follows from our original stipulation that the increments of magnitude of $\vec{H}_{ext}$ are associated with changes of orientation sufficient to ensure that the succession of flux sheets nucleated at the surface are super critical as regards to orientation. In other words, here, the rotation of $\vec{H}_{ext}$ generates a current density along the surface with $j_{\|} > j_{c\|}$. The observations we report in the next chapter provide strong evidence that a breathing mode does indeed occur as $\vec{H}_{ext}$ is varied in magnitude and direction. The breathing mode, however, was introduced by Clem[10] to explain the observation of a longitudinal voltage along a ribbon of a type II superconductor carrying a steady (constant) critical current in a static longitudinal field.

In this steady state situation the magnitude and orientation of $\vec{H}_{ext}$ are fixed. The entire specimen is filled with a lattice of noncollinear sheets of flux lines in a supercritical state both with respect to orientation and the density gradient, thus, $j_{\|} > j_{c\|}$ and $j_{\perp} > j_{c\perp}$. The time average of the magnitude and orientation of the

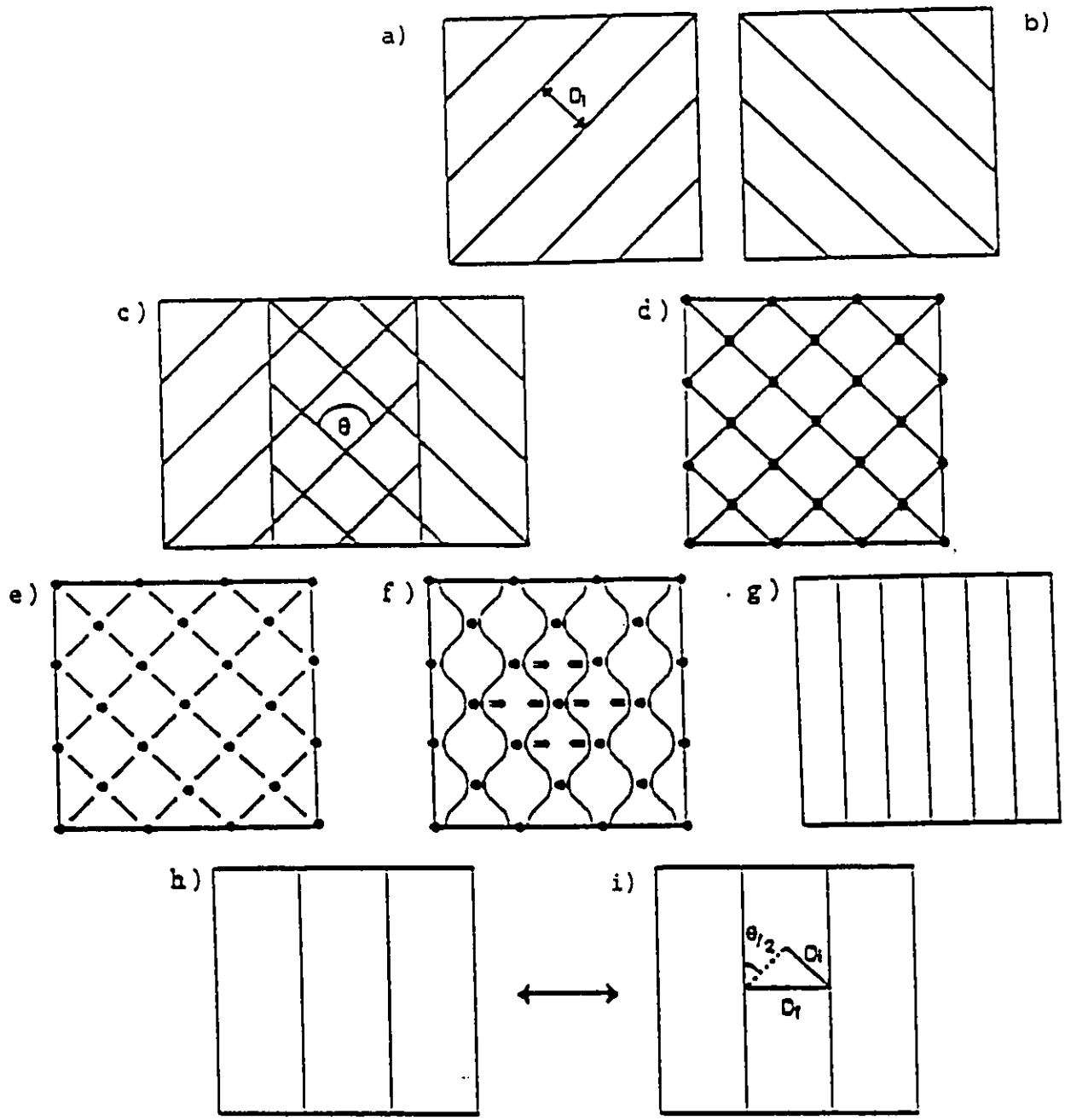

Figure 3.3: As described in the text, shows schematically the sequence of intersection, cross joining, straightening and separation of two sheets of flux lines.

magnetic flux density $\vec{B}(x)$ is constant. The component of $\vec{B}(x)$ perpendicular to the steady current I is however continously being consumed inside the specimen and replenished during the breathing in part of the cyclic events at the surfaces.

This can again be understood from consideration of Fig 3.3.(a),(b),(h) and (i). We now regard sheets (a) and (b) as entering at the opposite surfaces of the infinite slab and sheets (h) and (i) as representing two sheets subsequently leaving at the two surfaces after the process described above and displayed in (c),(d),(e),(f) and (g) has taken place. This simplified picture which focuses on only two sheets of flux lines grossly exaggerates the $\Delta\theta_c$ between the sheets but renders the essential features of the argument correctly.

The reader should note the following;

(i) The longitudinal flux is unchanged by the flux cutting process since the horizontal distance (along the y axis) between each flux quantum (flux line) remains fixed.

(ii) The net amount of transverse flux is also unchanged by the flux cutting process. It is evident that sheets (h) and(i) have no transverse flux. The net transverse flux carried by sheets (a) and (b) was also zero since the transverse component B_y of sheet (a) exactly cancels that of sheet (b). This transverse component was "consumed" (i.e. vanished by mutual annihilation) during the flux cutting process. An electric field E_{z1}, however was generated when sheet (a) moved inside the sample and an electric field E_{z2} was produced as sheet (b), (whose transverse component of magnetic flux density is opposite to that of sheet (a)) moved towards sheet (a). By the Josephson prescription $\vec{E} = \vec{B} \times \vec{v}$, E_{z1} and E_{z2} are both directed along the positive z axis, hence along the current density j_z.

The time average of $E_{z1}z$ or $E_{z2}z$ gives rise to the steady state flux flow voltage. $E_{z1}j_z$ accounts for the energy dissipation associated with this flux flow voltage and the fractional resistivity in the superconducting state.

In reality, many sheets of flux lines occupy the space between sheet (a) at the upper surface of the slab and sheet (b) at its lower surface. We recall that for such a configuration to occur, a steady transport current must be flowing along the z (vertical) axis throughout the volume of the specimen and a static externally applied magnetic field H_{ext}, also directed along the z axis must be present. The change of direction between adjacent sheets of flux lines will be much smaller than depicted in Fig. 3.3. The surface sheets, however, at nucleation will correspond to that shown in Fig 3.3 (a) and (b). The difference of direction between a sheet of flux lines entering ("breathing in" mode) and exiting ("breathing out" mode) at one surface will therefore be much smaller than sketched in Fig 3.3. The complete annihilation of the horizontal (y axis) component of the magnetic flux density entering from the two opposite surfaces therefore involves the participation of all the sheets in the slab for its final execution. As a consequence, the electric fields, hence flux flow voltage, predicted by this model is small compared with observations.

In part to resolve this problem of the magnitude of the flux flow voltage predicted by the "single flux cutting" just described, Clem[15] has proposed a "Double Flux Cutting Model". The detail of the sequence of events involved in this process are somewhat intricate. The essential result of the process however is that two adjacent non parallel sheets of flux lines such as shown in Fig 3.3 (a) and (b), effectively exchange position hence cross each other. This process requires a larger current density j_z than the single flux cutting mechanism.

It can readily be appreciated that sheet (a) of Fig. 3.3 after having "traded" place with sheet (b) will subtend a very supercritical angle with the neighbouring sheets of a non parallel flux line lattice. Consequently it will easily undergo double flux cutting through such a lattice until it emerges at the other surface of the slab. Simultaneously, flux sheets nucleated at that opposite surface and carrying a "negative" B_y component will be travelling in the opposite direction through the slab (i.e. towards the reader)

via double flux cutting sequences.

In this picture then, in the steady state, two sub lattices of non parallel flux lines are continuously traversing each other and flowing in an opposite direction throughout the specimen. The "breathing in" and "breathing out" modes still take place at the surfaces. The crucial difference is that now, the flux lines ejected during the "breathing out" possess the orientation of those entering at the opposite surface. This important feature together with the associated enhancement in the rate at which the tilted sheets exchange place, leads to good quantitative agreement with observed flux flow voltages in the flux cutting regime.

The fascinating scenarios we have just described have, unfortunately, remained inaccessible to "direct" experimental scrutiny and verification. Neutron scattering is the only probe available for the study of the structure of flux line lattices inside type II superconductors. This technique however can only provide information on the arrangement of parallel flux lines in the stationary state. Our experiment is the first attempt to "measure" and "test" the macroscopic consequences of the models just presented beyond the observation of flux flow voltages.

3.4 The Generalized Critical State

In the preceding sections we have outlined the accepted critical state concept which focuses on the migration of parallel flux lines in type II superconductors as they undergo depinning in response to a Lorentz driving force $\vec{F}_L = \vec{j} \times \vec{B}$. This leads to critical B profiles and associated critical current densities j_c in the material as the transport current is impressed and/or the external magnetic field is slowly varied. We have also described briefly scenarios proposed for the interaction, cutting, reconnection and cross-flow of non parallel flux lines. Clem and his collaborators have developed a quasi-macroscopic theoretical framework which incorporates these vari-

ous ideas phenomenologically. This theory is fundamental and its basic features are unassailable since it rests on Maxwell's equations. We now sketch this approach.

Firstly, the magnetic flux density vector $\vec{B}(x)$ is chosen as the appropriate frame of reference to describe the behaviour of the electrodynamic quantities. Thus, they write,

$$\vec{B} = \hat{\alpha}B \tag{3.9}$$

where the unit vectors $\hat{\alpha}$ and $\hat{\beta} = \hat{\alpha} \times \hat{x}$ express the direction of $\vec{B}$ with respect to the laboratory coordinates. Consequently, the electric field vector $\vec{E}$ comprises a component $E_{\parallel}$, parallel and a component $E_{\perp}$, perpendicular to $\vec{B}$. Similarly, the current density vector $\vec{j}$, comprises a component $j_{\parallel}$, parallel and a component $j_{\perp}$, perpendicular to $\vec{B}$. For planar geometry, in the frame of reference of $\vec{B}$, the Maxwell-Ampere equation $\nabla \times \vec{B} = \mu_o \vec{j}$ then reads,

$$\mu_o j_{\perp} = -\frac{dB}{dx} \tag{3.10}$$

$$\mu_o j_{\parallel} = B\frac{d\alpha}{dx} \tag{3.11}$$

Also for planar geometry, the Maxwell-Faraday equation $\nabla \times \vec{E} = -\partial\vec{B}/\partial t$ now reads,

$$\frac{\partial \vec{B}}{\partial t} = -\frac{\partial E_{\perp}}{\partial x} - E_{\parallel}\frac{\partial \alpha}{\partial x} \tag{3.12}$$

$$B\frac{\partial \alpha}{\partial t} = \frac{\partial E_{\parallel}}{\partial x} - E_{\perp}\frac{\partial \alpha}{\partial x} \tag{3.13}$$

These coupled differential equations must be solved exploiting the usual physical constraints that $E_{\parallel}(x)$, $E_{\perp}(x)$ and $B(x)$ must be continuous. Generally $\vec{B}$ at the surfaces of the specimen is an experimental variable known to and controlled by the researcher, hence this boundary condition is exploited to "initiate" solution of the differential equations. In our work, however, we will see that although $\vec{B}$ is known at the surfaces, its magnitude and direction in the cavity of the cylinder is not dictated by the observer. This feature introduces a major difficulty in the application of the

equations to the analysis of our results. In many situations of interest, a surface can be identified where from symmetry considerations, $E_\perp = 0$ and $E_\parallel = 0$. Unfortunately, such a surface does not appear or cannot readily be identified in our work.

Flux line depinning and flux line cutting enter the picture via two requirements, namely that,

$$E_\perp j_\perp \geq 0 \quad and \quad j_\perp \geq j_{c\perp} \tag{3.14}$$

where an electric field $E_\perp$ appears, and

$$E_\parallel j_\parallel \geq 0 \quad and \quad j_\parallel \geq j_{c\parallel} \tag{3.15}$$

where an electric field $E_\parallel$ appears.

These empirical requirements express the facts that flux line depinning and flux line cutting dissipate energy and are independent processes. We note that these two separate requirements constitute the essential, new and specific features of the theory. This double constraint contrasts with the less stringent requirement that $\vec{E} \cdot \vec{j} \geq 0$ when dissipation of energy occurs.

Consequently four different zones or regions can appear as a type II superconductor is subjected to external magnetic fields which vary in magnitude and direction.

- **(T zones)** Where only flux transport occurs. Here $E_\perp j_\perp > 0$, $j_\perp \geq j_{c\perp}$
- **(C zones)** Where only flux line cutting occurs. Here $E_\parallel j_\parallel > 0$, $j_\parallel \geq j_{c\parallel}$
- **(CT zones)** Where both flux transport and flux cutting occur, hence $E_\perp j_\perp > 0$, $j_\perp \geq j_{c\perp}$, $E_\parallel j_\parallel > 0$, $j_\parallel \geq j_{c\parallel}$
- **(O zones)** Zones where no energy dissipation takes place, hence $E_\perp = 0$, $E_\parallel = 0$. In these O zones, however, persistent current densities $j_\parallel \leq j_{c\parallel}$ and/or $j_\perp \leq j_{c\perp}$ can exist. Of course, electric fields $E_\perp$ and/or $E_\parallel$ were present when these were established.

The critical state model, developed some 30 years ago by Bean, London, Kim and Anderson (currently referred to as the Bean model) envisaged T and O zones

only. LeBlanc and his coworkers introduced CT zones over a decade ago on empirical grounds. The Generalized Critical State Model has added a new type of zone, the pure cutting regions (C zone) and embodied all of these ideas in a solid, unified and physical framework.

We have applied this framework to the analysis of data where planar geometry can be exploited and the boundary conditions are dictated by the experimenter. An analysis of our observations using this theory presents formidable difficulties. Firstly, the coupled equations are an order of magnitude more difficult to manipulate for cylindrical geometry. Even Clem and his theoretical team have yet to publish calculations for cylindrical geometry. Secondly, a cylindrical surface where $E_{\parallel} = 0$ and/or $E_{\perp} = 0$ does not occur when our specimen is filled with persistent currents. Finally, the quantity we need to predict from the theory is the behaviour of the magnetic flux density along the inner surface of the hollow cylinder. Usually, however, the boundary conditions determine the solution of the problem. Here we are confronted with finding a crucial boundary condition from a knowledge of one of its components (the azimuthal field inside the cavity). This is clearly a daunting and unusual challenge.

Chapter 4

Experimental Results

4.1 Introduction

As indicated in the previous chapter, all models proposed for the process of flux line cutting and interconnection visualize that even in the steady state, there will be considerable traffic of flux lines across the surfaces of the specimen. Whether "single" or "double" flux cutting events are thought to take place, flux lines will alternately enter and leave at the surfaces. Further, the orientation of the flux lines which enter will differ from those which leave. In all circumstances, the flux lines entering will have the orientation of the ambient magnetic flux density B_{ext}. In the steady state, this orientation is fixed, hence the flux lines nucleating and entering the surfaces will not vary in direction as time progresses. Consequently, the flux lines exiting, in order that the steady state be maintained, must emerge at a constant orientation. Through the mechanism of flux line cutting (single or double or otherwise), however, the ingoing and outgoing flux line sheets or lattices will be tilted with respect to each other.

Clearly it is desirable and important to design experiments which test and verify these ideas. This was the central purpose of our project. We believe that our

observations provide strong support for a breathing mode phenomenon where: (i) flux lines alternately or simultaneously enter and leave across a surface of a type II superconductor, hence a two way or cross flow takes place and (ii) the flux lines entering differ in orientation from that leaving the specimen. In our experiment, the physical quantity which monitors the net traffic of flux lines across the inner surface of the hollow cylinder is, $B_{z\,hole}$, the "level" of axial flux density in the cavity of the specimen. The cavity is a reservoir of finite and known dimension. If the "level", i.e. $B_{z\,hole}$, is seen to rise in the reservoir, then more axial flux is entering the reservoir than leaving it. If the "level is seen to drop in the reservoir, then more axial flux is leaving than entering. Clearly, if there is no traffic or no net exchange of axial flux between the cavity and the surrounding volume, (the wall of the hollow cylinder), the level of axial flux density will remain fixed. Also if only one way traffic is taking place, the level in the reservoir will drop if axial flux is being pumped out and rise if axial flux lines are being released into it. In our set up, $B_{z\,hole}$, the axial flux density is continuously monitored via a pickup coil placed in the cavity and feeding an operational amplifier-integrator.

It is of great interest to follow the changes in the configuration of the magnetic flux density in the wall which accompany the ebb and flow of $B_{z\,hole}$. Consequently, both the spatial average of the azimuthal and axial components of the magnetic flux density in the wall, $< B_\phi >_{wall}$ and $< B_z >_{wall}$ should be continuously monitored simultaneously with $B_{z\,hole}$. The evolution of these two quantities in unison with the rise and fall of $B_{z\,hole}$ provides important data for a detailed quantitative analysis of the phenomena under scrutiny. In particular, these data yield information on the dependence of $j_{c\|}$ on B. We stress, however, that the intricacies of the evolution of these two quantities ($< B_z >_{wall}$ and $< B_\phi >_{wall}$) plays no specific role in the qualitative interpretation of the observations.

4.2 "Classical" Expectations

4.2.1 Introduction

It is useful for a good understanding and full appreciation of the meaning of our observation to first examine the behaviour predicted in the "classical" framework (still subscribed to by many workers) where flux line cutting and cross flow does not occur.

It is universally accepted that as $\vec{H}_{ext}$ is made to increase in magnitude beyond H_{c1}, flux lines are caused to nucleate at the surface and enter the adjacent volume of type II superconductors with their orientation directed along $\vec{H}_{ext}$ at the time of nucleation. It is generally believed and well confirmed experimentally that each flux line carries a quantum of flux. This unit however plays no specific role in the interpretation of our observations. The crucial feature is that the quantum of flux entering the specimen is provided by the source of $\vec{H}_{ext}$. Therein lies the novel and crucial aspect of our experiment. In our set up, when the hollow cylinder is superconducting, the source of axial magnetic flux, nucleating and penetrating along the inner surface of the wall, is the enclosed finite axial flux,

$$\Phi_z = B_{z\,hole}\,\pi R_i^2 \tag{4.1}$$

Every quantum of axial flux "pumped" into the wall across this surface removes that amount from Φ_z hence depresses $B_{z\,hole}$. Conversely, every quantum of axial flux released by the wall across this surface augments Φ_z hence raises $B_{z\,hole}$.

In our experiment, the "external" magnetic field along the inner surface of the long hollow cylinder, reads,

$$\vec{H}(R_i) = \hat{\phi} H_\phi(R_i) + \hat{z} H_z(R_i) \tag{4.2}$$

where we have assumed idealized cylindrical geometry. In reality, end effects (demagnetization factor along the z axis) will cause the "external" magnetic field inside

the cavity and around the hollow cylinder to be nonuniform. We do not envisage that this feature will qualitatively affect the observed phenomena. To minimize the influence of the finite length of our specimen on the quantitative data, we have made the pickup coils (both the inner and outer) a fraction of the length of the specimen. Consequently we consider $B_{z\,hole}$ to be uniform and take,

$$< B_{z\,hole} >= \mu_o H_z(R_i) = B_{z\,hole} \tag{4.3}$$

In our work, the external magnetic field is usually helical, hence the flux lines which are nucleated are helical. It is generally accepted that, unless flux cutting processes intervene, helical flux lines migrate radially only across the wall of the superconducting hollow cylinder. Consequently, the pitch P and the helicity n_c of a cylindrical sheet of flux lines is regarded as constant as the sheet expands or contracts in radius during its radial displacement. Following standard practice we write;

$$P = \frac{1}{2\pi n_c} = \frac{r\,B_z(r)}{B_\phi(r)} = \frac{r\,H_z(r)}{H_\phi(r)} \tag{4.4}$$

where n_c is the number of circuits a flux line makes around the circumference of the wall per unit length along the z axis (see Fig 4.1).

4.2.2 H_ϕ impressed

We now focus on the situation established in a first phase of our investigations. Here the cylinder is first allowed to become superconducting by cooling from above T_c to 4.2K in a static axial magnetic field $H_\parallel$ (Field Cooling). We stress that $H_\parallel$ provided by the long solenoid is maintained fixed throughout each measurement. Our system can maintain $H_\parallel$ constant to better than one part in a thousand. We stress however that the behaviour we examine is immune to all minor drifts. Giant drifts $\Delta H_\parallel \approx H_*$, the full penetration field ($\mu_o H \approx 20mT$), can however have an effect on the qualitative aspects of our observations. This danger then is several orders of magnitude away from perturbing our study.

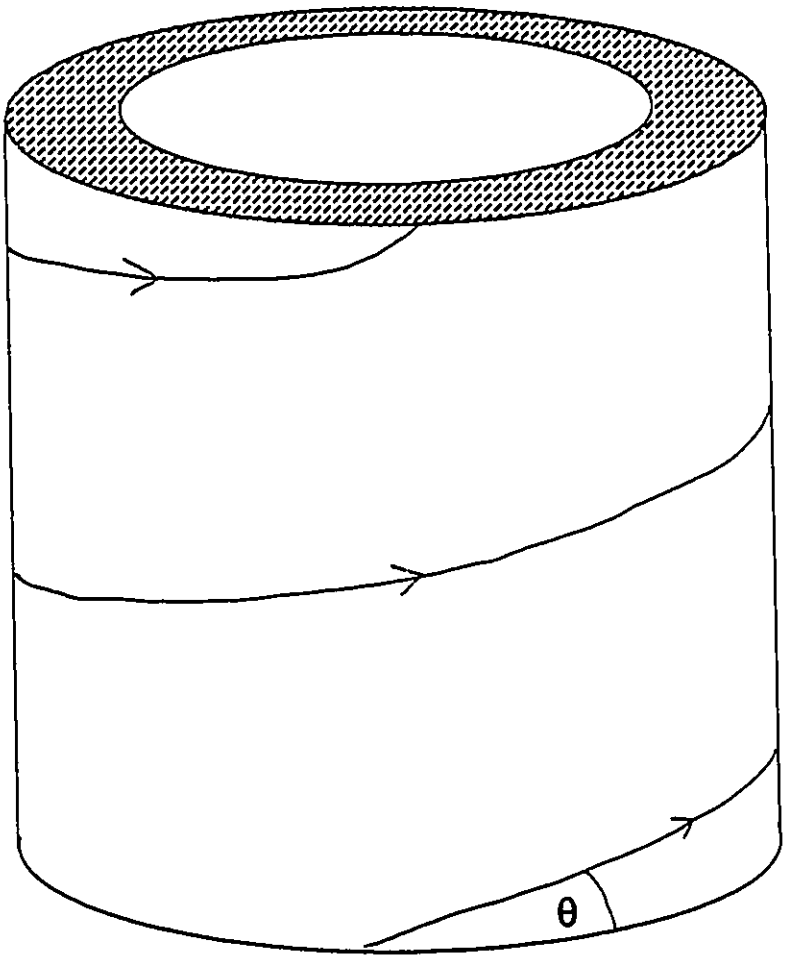

$$P = \frac{1}{2\pi n_c}$$

Figure 4.1: Example of helical flux line with $n_c = 2$. Pitch, P, is "classically" expected to remain constant as it migrates radially, however, its tangential angle, θ, will change with radius r.

After field cooling, the specimen is threaded by straight flux lines permeating its volume nearly uniformly and all directed longitudinally. The mutual repulsion of these flux lines is sufficient to overcome the pinning strength of our specimen, hence some flux lines are expelled from the wall during the field cooling. Some of these flux lines are expelled into the cavity, causing $B_{z\,hole}$ to rise above $\mu_o H_\parallel$. This manifestation of Abrikosov diamagnetism (the Meissner Effect in type II superconductors) is expected and only "shifts" the initial baseline for our observations. In the strong pinning hollow cylinder studied by Fillion and Golebiowski, this feature was absent.

$\vec{H}(R_i)$ is now made to increase in magnitude and simultaneously tilted along the $\hat{\phi}$ (azimuthal) axis. Concurrently $\vec{H}(R_o)$ along the outer surface also rises in magnitude and is tilted. Since,

$$H_\phi(R_i) = \frac{nI}{2\pi R_i}, \qquad H_\phi(R_o) = \frac{NI}{2\pi R_o} \tag{4.5}$$

It is clear from the definitions of pitch and helicity (eqn 4.4) that, the flux lines nucleated along R_i are more helical than those nucleated along R_o, since,

$$\frac{n_c(R_i)}{n_c(R_o)} = (\frac{R_o}{R_i})^2 \frac{B_{z\,hole}}{\mu_o H_\parallel} \tag{4.6}$$

and $B_{z\,hole} \approx \mu_o H_\parallel$

Now the following scenario is universally accepted; (i) Every helical flux line nucleated along the inner surface R_i removes a quantum ϕ_o of axial flux from the cavity and transfers it to the wall. This helical flux line also injects $n_c(R_i)\phi_o z$ of azimuthal flux in the wall of length z. (ii) Every helical flux line nucleated along the outer surface R_o adds one quantum of axial flux to the wall and also injects $n_c(R_o)\phi_o z$ of azimuthal flux.

In the absence of flux cutting processes the lattice of straight longitudinal flux lines initially permeating the wall will consequently be compressed into a smaller volume of the wall to make room for the immigration of the new flux lines entering

across the inner and outer surfaces. Consequently, the following developments are inexorably anticipated to take place simultaneously and are illustrated schematically in Fig 4.2. $B_{z\,hole}$ must drop monotonically as the axial flux the cavity contains is being transferred (pumped) into the wall. Meanwhile $< B_z >_{wall}$ and $< B_\phi >_{wall}$ will grow continuously. Thus, unless flux cutting or other processes intervene, these three courses of events will proceed undisturbed until the superconducting state is extinguished when H_{c2} is attained. At this juncture, the onset of the normal state will lead to an abrupt rise of the depressed level of axial flux in the cavity to the applied level $\mu_o H_\parallel$. Again we refer the reader to Fig 4.2.Also the large accumulated axial flux density in the wall will collapse to the ambient level $\mu_o H_\parallel$. Throughout all this history the application of H_ϕ via the toroidal magnet coil will have caused $< B_\phi >_{wall}$ to continuously increase. This quantity however is expected to always lag behind $\mu_o < H_\phi >$, the spatial average of the applied magnetic flux density,

$$\mu_o < H_\phi >= \frac{\mu_o N I}{2\pi(R_o - R_i)}\, ln(\frac{R_o}{R_i}) \tag{4.7}$$

A reason for this lag is the following. In the absence of flux line cutting, an annular region appears in which the initial population of longitudinal flux lines originally permeating all of the wall at the outset are being compressed. Thus without flux cutting processes, all of this flux line lattice must survive, although confined to and squeezed into a smaller and smaller but nevertheless finite space. The crucial feature is that, this space, whatever its radial dimension, is denied to occupancy by the helical flux lines which have invaded the wall as H_ϕ was impressed and caused,

$$\mid \vec{H}(R_i) \mid = \{\ H_\phi^2(R_i) + (\frac{B_z h}{\mu_o})^2\ \}^{1/2} \tag{4.8}$$

and

$$\mid \vec{H}(R_o) \mid = \{\ H_\phi^2(R_o) + H_\parallel^2\ \}^{1/2} \tag{4.9}$$

to grow to H_{c2}. The scenario we have just described then leads to the prediction of

Figure 4.2: Behaviour predicted in absence of flux line cutting

a rapid growth of $< B_\phi >_{wall}$ just as H_{c2} is approached (see Fig 4.2). In our work, we have not monitored the evolution of $< B_\phi >_{wall}$. However, related investigations on a material of similar weak pinning strength, Gandolfini et al[17] have observed behaviour opposite to that just described. In effect, they find that the lag of $< B_\phi >_{wall}$ below $\mu_o < H_\phi >$ is diminished rather than enlarged.

A glance at the data curves for $B_{z\,hole}$ and $< B_z >_{wall}$ displayed at the end of this chapter reveals that as $< H_\phi >$ is impressed, the behaviour just predicted is followed only over a portion of the sweep from 0 to H_{c2}. Clearly then, the thesis that helical flux lines retain their pitch and their integrity as they are made to migrate and are compressed in a type II superconducting material cannot be sustained.

4.2.3 H_ϕ Removed

In a second phase of our investigation the hollow cylinder is field cooled in the presence of a helical magnetic field whose magnitude is near but below H_{c2} for the ambient final temperature of 4.2 K. Consequently here, in the superconducting state, the wall of the specimen is permeated by a lattice of helical flux lines where the helicity n_c , initially varies across the radius of the wall according to the prescription,

$$n_c(r) = (\frac{R_o}{r})^2 \, n_c(R_o) \tag{4.10}$$

Now, the magnitude of "$\vec{H}_{ext}$" (i.e. $\mid \vec{H}(R_i) \mid$ and $\mid \vec{H}(R_o) \mid$) is diminished gradually by reducing the azimuthal component of $\vec{H}_{ext}$ (i.e. $H_\phi(R_i)$ and $H_\phi(R_o)$). It is universally accepted that the diminution of $\mid \vec{H}_{ext} \mid$ will cause flux lines to be released from the wall unless surface barriers, hence surface currents, oppose such an occurrence. However, auxiliary measurements have indicated the absence of any significant surface barrier in our specimen in the range of fields present in these experiments. All workers agree that the escape of flux lines from the wall will lead to the development of "classical" critical state configurations advancing inwards from

the two surfaces.

Again, it is universally recognized that the release of a helical flux lines from the wall across its inner surface will remove one quantum of axial flux from the wall and transfer this amount to the axial flux already threading the cavity thereby causing $B_{z\,hole}$ to rise and $< B_z >_{wall}$ to fall. Concurrently, the departure of a helical flux line from the wall across its outer surface will remove one quantum of axial flux from the wall, thereby also contributing to the decline of $< B_z >_{wall}$. (The longitudinal flux outside the cylinder however remains at $H_{\|}$ maintained by the surrounding solenoid. In a sense, the universe outside the sample can be regarded as an infinite reservoir).

The accepted views then, unless other processes or events come into play, inexorably predict that, (i) $B_{z\,hole}$ will grow monotonically and (ii) concomitantly, $< B_z >_{wall}$ will diminish monotonically, as H_ϕ descends to zero. Again a glance at all the pertinent data curves displayed at the end of the chapter reveals that the behaviour predicted by the "classical" ideas is indeed observed over the initial portion of the reduction of "H_{ext}". However, at some stage in the diminution of "H_{ext}", the expected evolution ceases and the trends subsequently exhibit a complete 180° reversal from that just predicted. Now $B_{z\,hole}$ rather than rising is seen to descend and $< B_z >_{wall}$ instead of continuing to drop is observed to ascend.

4.3 Interpretation of our Results

Clearly, the observed behaviour is in drastic disagreement with "classical" expectations. We will now scrutinize these "unexpected" turn of events, where trends opposite to that anticipated in the absence of flux line cutting are seen to appear. In Figs 4.3 to 4.6, the segments labelled A2 and C indicate the zones where the behaviour is in harmony with the "classical" picture. The sections labelled A1, B and D, indicate the regions where the evolution of $B_{z\,hole}$ (and to some extent $< B_z >_{wall}$) evolves in

opposition to the "traditional" picture where flux lines preserve their integrity and separate existence. We will argue that the "retrograde" behaviour provides evidence for a breathing mode, in other words for an exchange of flux between the wall and the cavity, hence a cross flow or counter flow or two way traffic across the inner surface of the wall. Presumably, for consistency, the events taking place along the inner surface of the wall are also occurring along the outer surface. In our set up, however, we are not equipped with a sensor or gauge to monitor the complete traffic of flux lines across the outer surface. Consequently, we can only surmise from considerations of symmetry and consistency that the behaviour there duplicates that witnessed at the boundary with the cavity where $B_{z\,hole}$ directly measures the net traffic of axial flux.

Our central task or challenge is to account for, (i) a rise in $B_{z\,hole}$ along the segments labelled A1 and B in the figures at the end of the chapter in spite of the fact that the magnitude of "H_{ext}" is pumping axial flux out of the cavity and, (ii) a drop in $B_{z\,hole}$ along the segment labelled D in the figures, although a decrease in the magnitude of "H_{ext}" is releasing axial flux from the wall into the cavity. In other, perhaps more colourful but nevertheless accurate, words, we need to explain, (i) why the reservoir is filling up while the "pump" (the increase in $\mid \vec{H}(R_i) \mid$) is acting to empty it and (ii) how the reservoir can be emptying when the surrounding wall is pouring magnetic flux into it.

To understand these phenomena we must bear in mind that a helical flux line carries only one quantum of axial flux but contributes an amount $n_c\phi_o z$ to the azimuthal flux in the wall of the cylinder. n_c can vary from zero for pure longitudinal flux lines to large values when $B_\phi >> B_z$.

The entry of $\Delta N_{\_}$ helical (or longitudinal) flux lines into the cavity will cause the axial flux it contains to rise an amount,

$$\Delta\Phi'_{z\,hole} = \Delta B'_{z\,hole}\,\pi\,R_i^2 = \Delta N_{\_}\,\Phi_o \qquad (4.11)$$

where the arrow $\leftarrow$ points towards the axis of the cylinder and indicates flux lines leaving the wall and entering the cavity. Conversely a decrease $\Delta\Phi''_{z\,hole}$ of the axial flux in the cavity will occur when $\Delta N_{\rightarrow}$ helical (or longitudinal) flux lines are nucleated at R_i,

$$\Delta\Phi''_{z hole} = \Delta B''_{z\,hole}\,\pi\,R_i^2 = \Delta N_{\rightarrow}\,\Phi_o \tag{4.12}$$

where the arrow $\rightarrow$ pointing away from the axis indicates flux lines leaving the cavity and entering the wall.

Visualizing that a two way traffic of flux lines can simultaneously or alternately be taking place across the inner surface of the wall ("breathing" mode or other process) we then write,

$$\begin{aligned}
\Delta\Phi_{z\,hole} &= \Delta\Phi'_{z\,hole} - \Delta\Phi''_{z\,hole} \\
\Delta\Phi_{z\,hole} &= (\Delta B'_{z\,hole} - \Delta B''_{z\,hole})\pi R_i^2 \\
\Delta\Phi_{z\,hole} &= \Delta B_{z\,hole}\pi R_i^2
\end{aligned}$$

$$\Delta\Phi_{z\,hole} = (\Delta N_{\leftarrow} - \Delta N_{\rightarrow})\Phi_o \tag{4.13}$$

Clearly an increase (decrease) of the axial magnetic flux in the cavity is accompanied by a corresponding decrease (increase) in the axial flux permeating the wall.

Turning now to the net change in the azimuthal flux permeating the wall corresponding to the flux line traffic across R_i visualized above, we can write,

$$\Delta\Phi_{\phi\,wall} = \Delta < B_\phi >_{wall} (R_o - R_i)\,z$$

$$\Delta\Phi_{\phi\,wall} = (n_c^{\rightarrow}\,\Delta N_{\rightarrow} - n_c^{\leftarrow}\,\Delta N_{\leftarrow})\,z\Phi_o \tag{4.14}$$

where $n_c^{\leftarrow}$ and $n_c^{\rightarrow}$ denote the helicity of the flux lines entering and leaving the cavity hence leaving and entering the wall.

Concurrently the traffic of flux lines across the outer surface of the cylinder will contribute to the net change in the axial and azimuthal flux threading the wall. Consequently we can write,

$$\Delta\Phi'_{z\,wall} = (\Delta N'_{\leftarrow} - \Delta N'_{\rightarrow})\,\Phi_o \tag{4.15}$$

and,

$$\Delta\Phi'_{\phi\,wall} = (n_c^{\leftarrow}\Delta N'_{\leftarrow} - n_c^{\rightarrow}\Delta N'_{\rightarrow})\,z\,\Phi_o \tag{4.16}$$

where we use the single primes to indicate the link with the outer surface and the arrows $\leftarrow$ and $\rightarrow$ continue to indicate the direction of the "traffic" towards or away from the axis of the cylinder and the corresponding helicity.

The total increment (decrement) of axial and azimuthal flux in the wall will evidently consist of the combination of the two appropriate net contributions from the traffic across the two surfaces. We focus on equations (4.13) and (4.14) because they contain the essential elements of our explanation of the observed behaviour.

When $\vec{H}_{ext}$ hence $\mid \vec{H}(R_i) \mid$ is growing in magnitude, $\Delta\Phi_{\phi\,wall}$ is known to be increasing (this behaviour is universally acknowledged and has been experimentally verified in our set up by Fillion[16] and Golebiowski[18]). Turning to equation (4.14) this means that

$$n_c^{\rightarrow}\Delta N_{\rightarrow} > n_c^{\leftarrow}\Delta N_{\leftarrow} \tag{4.17}$$

If $\Delta B_{z\,hole}$ is seen to rise as in the regions labelled A1 and B in the figures, we must conclude from equation (4.13) that

$$\Delta N_{\leftarrow} > \Delta N_{\rightarrow} \tag{4.18}$$

Clearly equations (4.15) and (4.16) can then only be satisfied if,

$$\frac{n_c^{\rightarrow}}{n_c^{\leftarrow}} > \frac{\Delta N_{\leftarrow}}{\Delta N_{\rightarrow}} > 1 \tag{4.19}$$

Equation (4.19) signifies that the helicity of the flux lines entering the wall from the cavity is sufficiently greater that that emerging from the wall into the cavity to overcome the fact that now, as observed by the rise in $B_{z\,hole}$, more flux lines are entering the cavity than are being pumped out of it. It is beyond the scope or purpose of this thesis to develop in any detail the physical reason for the occurrence of this "imbalance". Our central point is that our experiment reveals that such and imbalance can occur and can be accounted for by equations (4.13) and (4.14). We stress that these equations are simple statements based on the concept of two way flow (cross flow, counter flow or breathing mode) across the surface R_i.

It is a straightforward matter to apply equations (4.13) and (4.14) to the behaviour encountered when $\vec{H}_{ext}$ is being diminished in magnitude, (hence $< H_\phi >$ removed), thus to the regions labelled D in the figures. In these circumstances, equation (4.14) dictates that,

$$n_c^{\rightarrow}\Delta N_{\rightarrow} < n_c^{\leftarrow}\Delta N_{\leftarrow} \tag{4.20}$$

and equation (4.15) requires that,

$$\Delta N_{\leftarrow} < \Delta N_{\rightarrow} \tag{4.21}$$

hence, equations (4.20) and (4.21) demand that,

$$\frac{n_c^{\leftarrow}}{n_c^{\rightarrow}} > \frac{\Delta N_{\rightarrow}}{\Delta N_{\leftarrow}} > 1 \tag{4.22}$$

Equation (4.22) is analogous to but the converse of equation (4.19). It accounts for the observation that along section D of the data curves, $B_{z\,hole}$ is declining although here the wall is releasing helical flux lines into the reservoir. Again, the key feature, is that this can occur if, (i) two way flow is taking place across R_i and (ii) the helicity of the flux lines ejected by the wall into the cavity is sufficiently larger than the helicity of the flux lines nucleated out of the cavity to compensate for the fact that, since $B_{z\,hole}$ is now decreasing, the number of flux lines leaving the reservoir must now be greater that that entering it.

The evolution of $< B_z >_{wall}$ accompanying the changes of axial flux density in the hole is displayed in the figures. An examination of these curves shows that they provide confirmation of our interpretation of the fascinating and unexpected behaviour encountered in the cavity. However, we do not expect that the reversals in the trends taking place in the wall will be exactly in phase with that occurring in the reservoir. The reason for this "phase shift", is that, while the reservoir has only one boundary (R_i) across which flux enters and leaves, the wall has two frontiers (R_i and R_o). Consequently, the net changes of flux in the wall are determined by the traffic of flux lines across both of its surfaces. Further, since the helicity and density of the flux lines along R_o differs from that along R_i at all times, it is not surprising that the ebb and flow of $< B_z >_{wall}$ does not proceed exactly in "unison" (albeit in opposite "direction") with that observed in the reservoir. We note nevertheless that, in accord with the picture we have proposed, generally, a rise in $< B_z >_{wall}$ is associated with a drop in $B_{z\,hole}$ and vice versa.

4.4 Conclusion

The evolution of $B_{z\,hole}$ the axial flux density in the cavity of a hollow cylinder is observed to deviate dramatically from the predictions of a "classical" framework where the traffic of flux lines across the surfaces of type II superconductors is thought to proceed along one direction only dictated by whether the magnitude of $\vec{H}_{ext}$ is increasing of decreasing. Our observations however provide strong support for the ideas that cylindrical sheets of helical flux lines can undergo cutting processes and thereby traverse each other, hence exhibit cross flow at the surfaces (breathing modes) and in the body of type II superconductors.

Heretofore, the idea of cross flow of sublattices of flux lines has been confined solely to steady state situations, namely, the flux flow voltage in a wire or ribbon

carrying a D.C. current in a static longitudinal $\vec{H}_{ext}$. Our experiment demonstrates that the cross flow and attendant breathing mode can take place in non steady state situations. Indeed, continuity and consistency suggest that the cross flow of flux lines may also be occurring along regions A2 and C of our data curves. In the circumstances prevailing along these regions, although cross flow may be taking place, it does not generate an "imbalance", hence a reversal in the evolution of $B_{z\,hole}$ and $< B_z >_{wall}$.

Finally we note that the onset of the deviations from "classically" predicted behaviour appear to correspond to the generation of a special saturated critical state configuration of the persistent currents in the wall of the cylinder. In this configuration, the azimuthal circulating currents associated with the change in $B_{z\,hole}$ relative to $\mu_o H_{\|}$ at the outer surface, are estimated to occupy the entire width of the wall. This conclusion follows from the observation that here, $\mid B_{z\,hole} - \mu_o H_{\|} \mid \approx B_*$ the full penetration field for the corresponding field ranges.

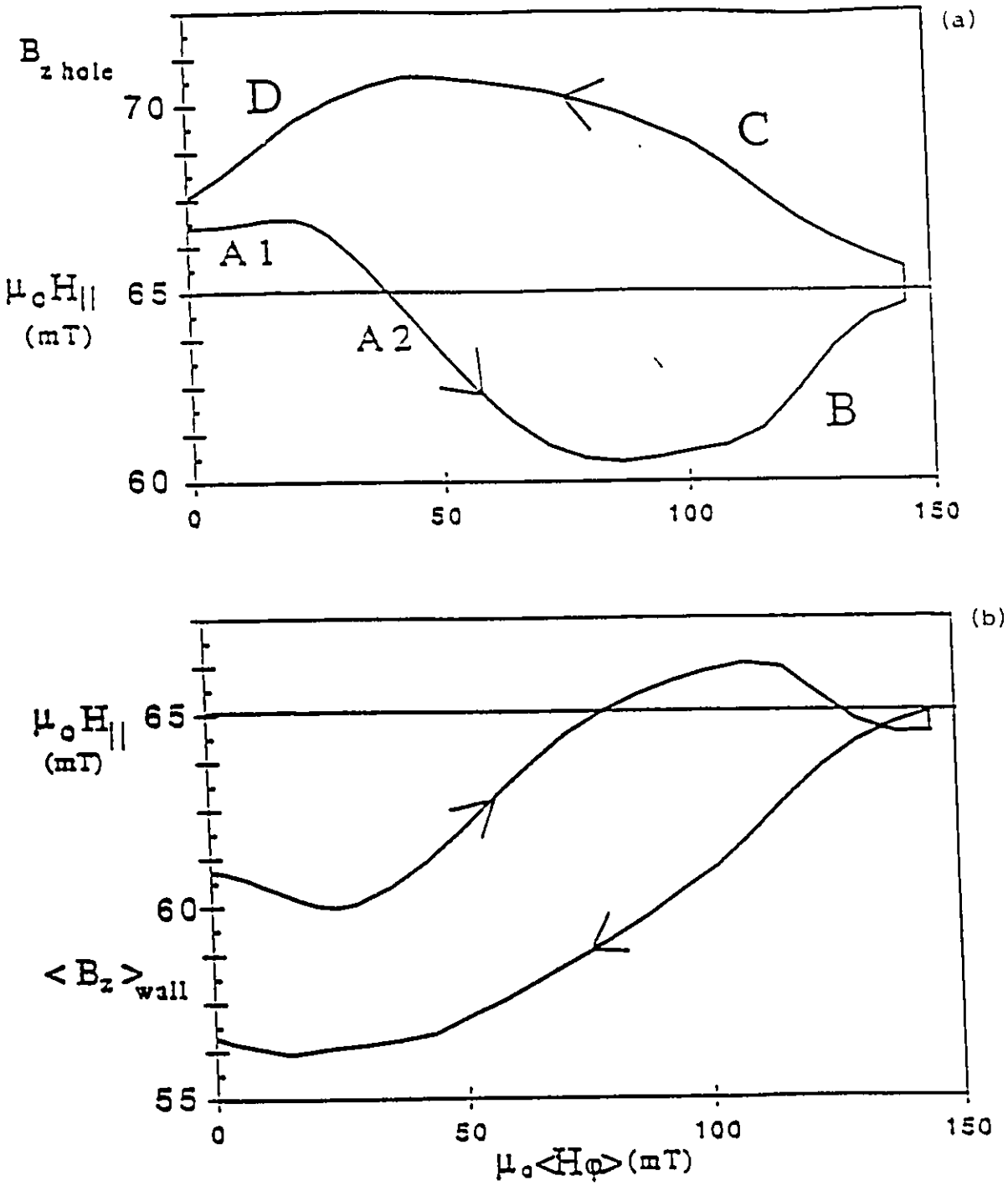

Figure 4.3: (a) Evolution of the axial magnetic flux density in the cavity vs $\mu_o < H_\varphi >$, the applied azimuthal magnetic flux density averaged over the cross section of the wall of the hollow cylinder. (b) Complement to (a), displaying the concomitant evolution of the spatial average of axial magnetic flux density in the wall of the hollow cylinder. Regions labeled A1, A2, B, C, and D are discussed in the text. Here $\mu_o H_\parallel = 65\,mT$.

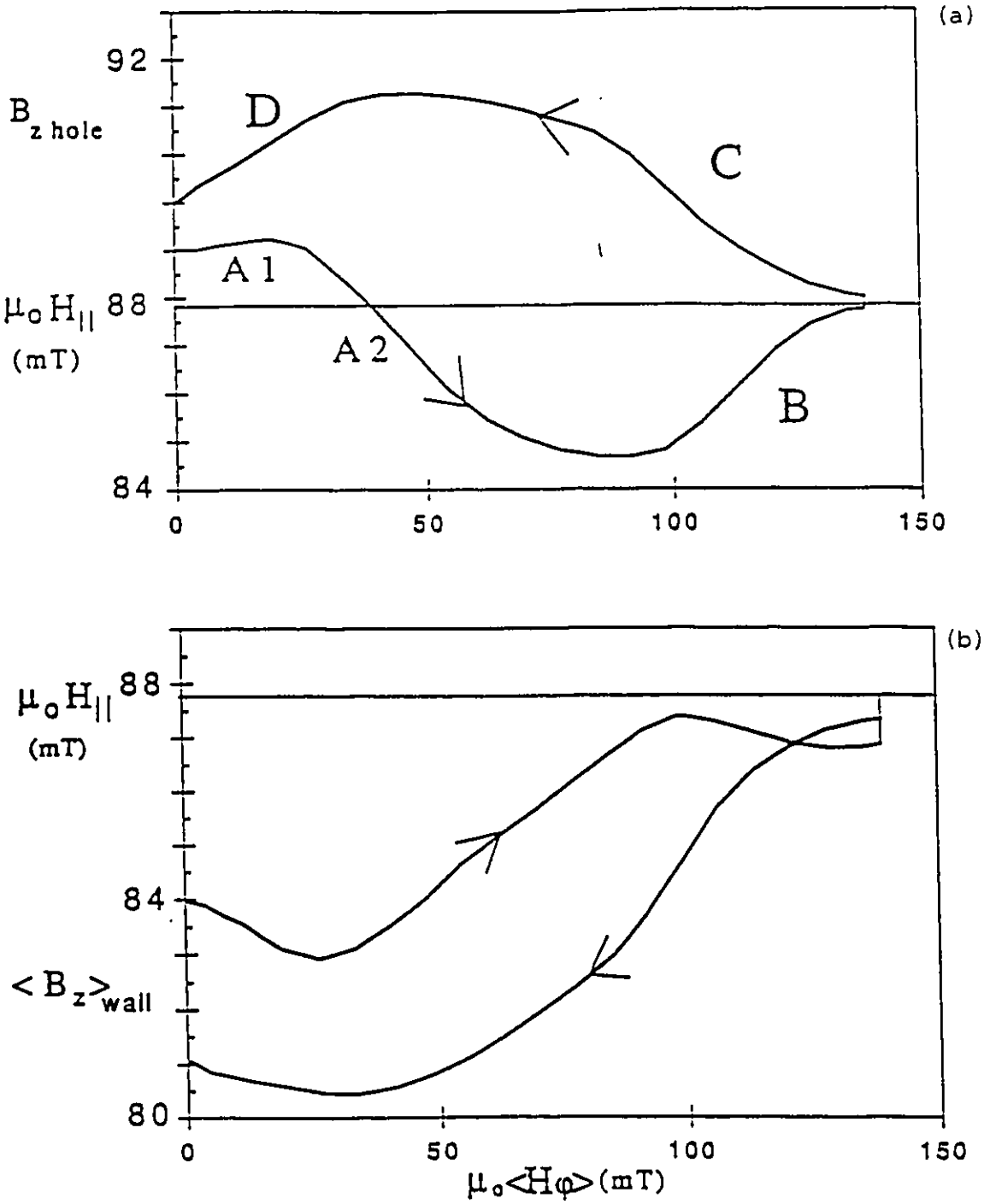

Figure 4.4: (a,b) As in Fig. 4.3 except here $\mu_o H_{||} = 87.8\,mT$.

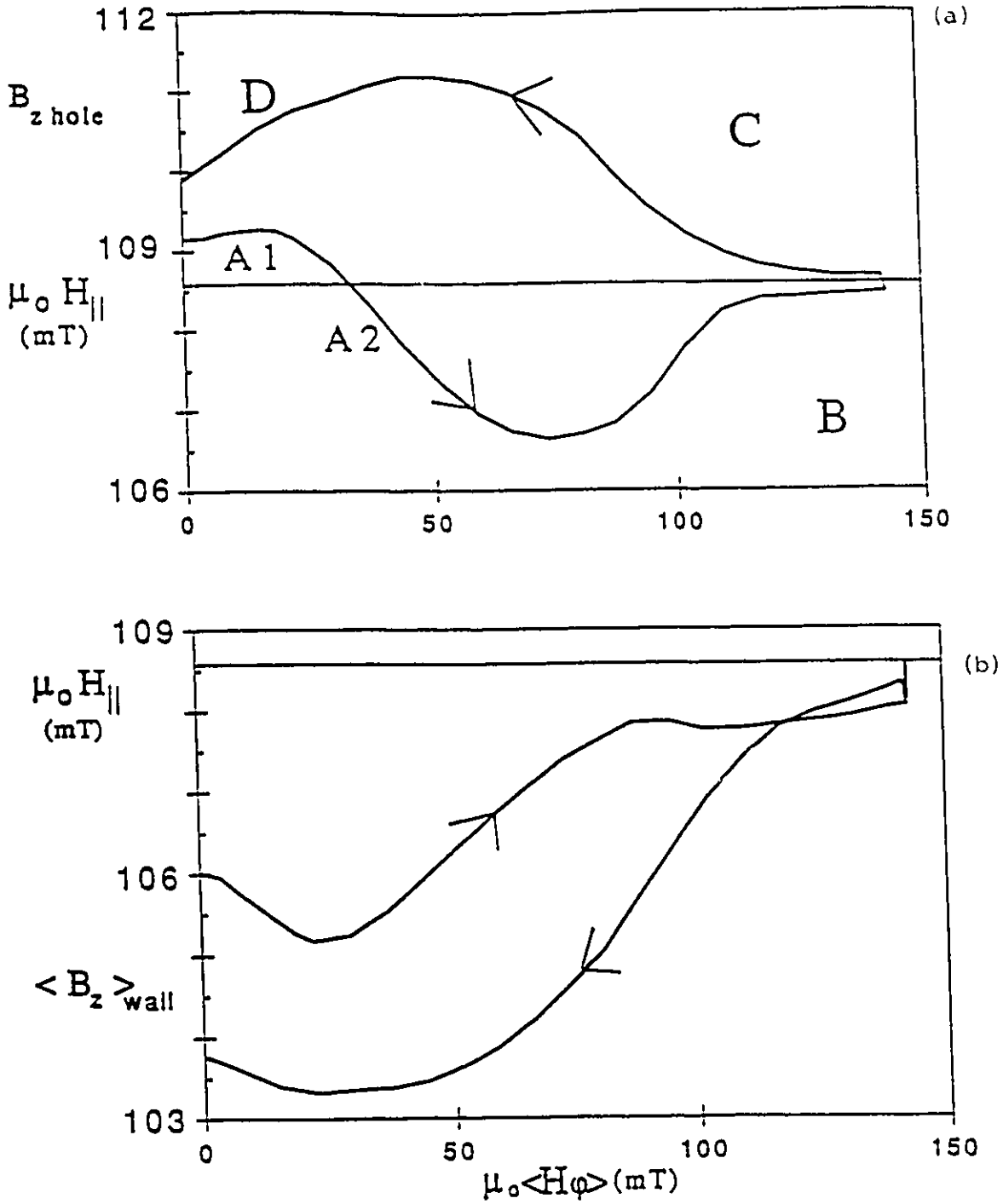

Figure 4.5: (a,b) As in Fig. 4.3 except here $\mu_o H_{||} = 108.6\,mT$.

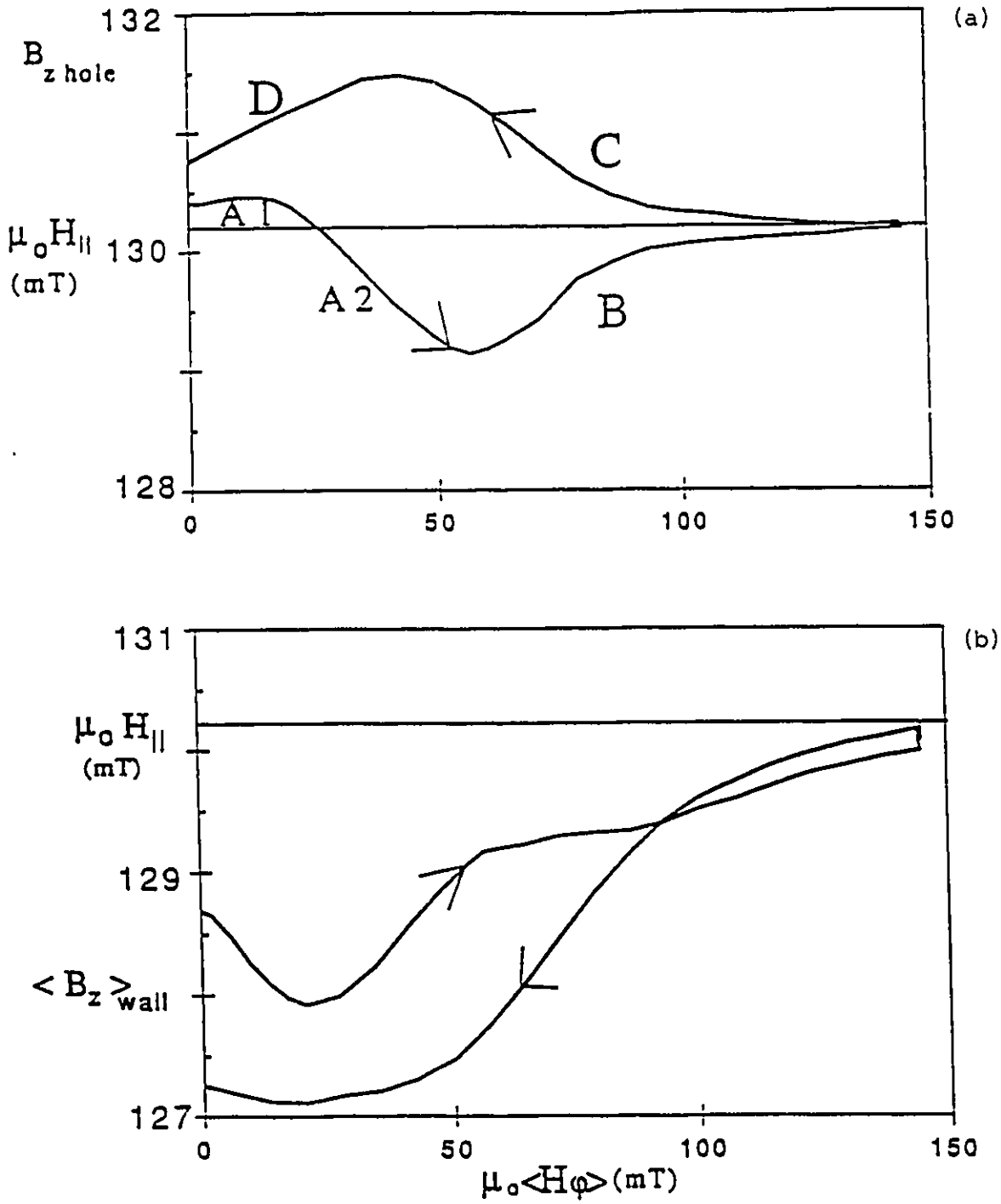

Figure 4.6: (a,b) As in Fig. 4.3 except here $\mu_o H_{||} = 130.2\,mT$.

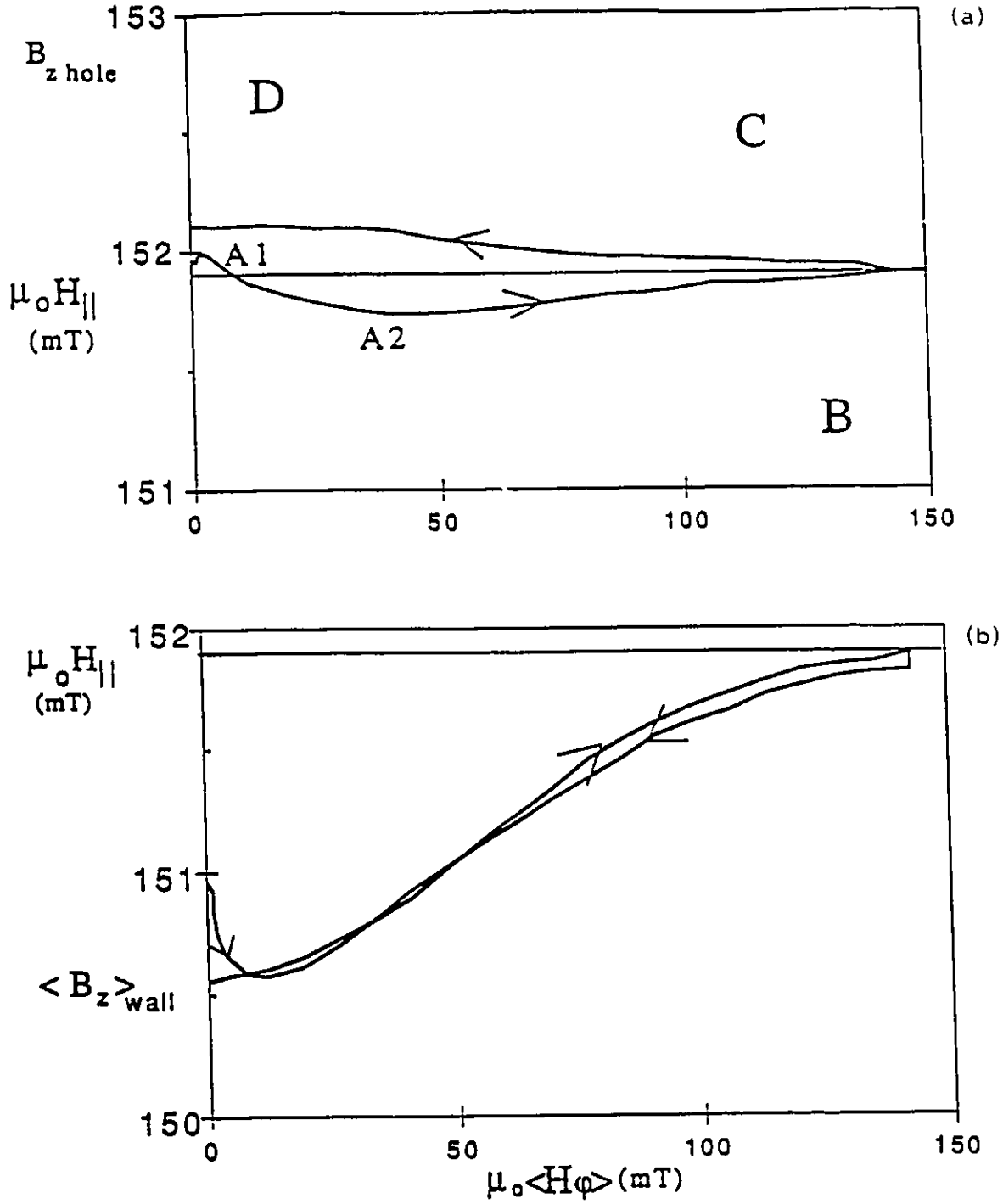

Figure 4.7: (a,b) As in Fig. 4.3 except here $\mu_o H_{\|} = 151.9\,mT$.

Bibliography

[1] A.A Abrikosov, *Soviet Physics JETP,* 5: 1174-1182, (1957)

[2] E.H. Brandt and A Sudbo, *Phys Rev Lett,* 66(17): 2278, (1991)

[3] E.H. Brandt, J.R. Clem and D.G. Walmsley, *J. Low Temp Phys,* 37(1/2): 43-55, (1979)

[4] E.H. Brandt *J. Low Temp Phys* 39: 41-61, (1980)

[5] E.H. Brandt *J. Low Temp Phys* 44: 59-72, (1981)

[6] E.H. Brandt *J. Low Temp Phys* 44: 33-57, (1981)

[7] A.M. Cambell and J.E. Evetts, *Critical Currents in Superconductors,* (Taylor and Francis, London, 1972), p.61

[8] J.R. Cave, J.E. Evetts and A.M. Campbell, *Journal de Physique (Colloque),* 39(C6): 614-616, (1978)

[9] L. Civale, A.D. Marwick, T.K. Worthington, M.A. Kirk, J.R. Thompson, L. Krusin-Ebaum, Y. Sun, J.R. Clem and F. Holtzberg, *Phys Rev Lett,* 67(5): 648-651, (1991)

[10] J.R. Clem,*J. Low Temp Phys,* 38(3/4): 353-370, (1980)

[11] J.R. Clem,*Phys Rev B,* 26(5): 2463-2473, (1982)

[12] J.R. Clem and S.Yeh, *J. Low Temp Phys*, **39**(1/2): 173-189 (1980)

[13] J.R. Clem *J. Appl Phys*, **50**(5): 3518-3530 (1979)

[14] J.R. Clem and A. Perez-Gonzalez,*Proceedings of the Int. Symp. on Flux Pinning and Electromagnetic Properties of Superconductors*, (1985)

[15] J.R.Clem *Physica* **107B**: 453 (1981)

[16] G. Fillion *Ph.d Thesis, University of Ottawa*, (1986)

[17] G. Gandolfini, M.A.R. LeBlanc and J. Sekerka *Cryogenics* **29**: 373-378, (1989)

[18] A. Golebiowski *M.Sc Thesis, University of Ottawa*, (1988)

[19] B.D. Josephson *Phys Rev*, **152**: 211 (1966)

[20] M.A.R LeBlanc, D. LeBlanc, A. Golebiowski and G. Fillion, *Phys Rev Lett*, **66**(25): 3309-3312, (1991)

[21] J.D. Livingston *Phys Rev*, **129** (5): 1943-1949 (1963)

[22] J.P. Lorrain, M.A.R. LeBlanc and A. Lachaine, *Can J. Phys*, **57**: 1458-1477 (1979)

[23] D.R. Nelson and H. S. Seung, *Phys. Rev. B* **39**: 9153 (1989); M. C. Marchetti and D. R. Nelson, *Phys. Rev. B* **41**: 1910 (1990)

[24] S. P. Obukhov and M Rubinstein, *Phys. Rev. Lett.* **65**: 1279 (1990)

[25] H.K. Onnes, *Commun Phys Lab Univ Leiden*, **120b**, (1911)

[26] A. Sudbo and E.H. Brandt, *Phys Rev Lett*, **67**(22):3176-3179, (1991)

[27] D.G. Walmsley, *J. Phys F***2**,: 510 (1972)